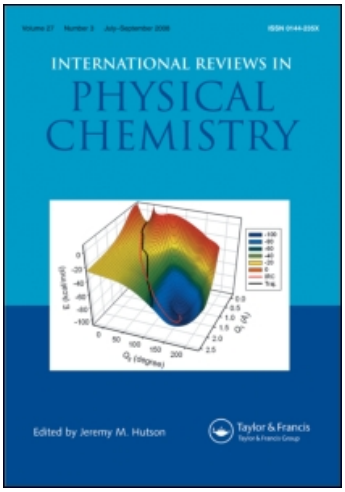

International Reviews in Physical Chemistry
Publication details, including instructions for authors and subscription information:
http://www.informaworld.com/smpp/title~content=t713724383

Coherent rotational excitation by intense nonresonant laser fields

Yasuhiro Ohshima[a]; Hirokazu Hasegawa[a]
[a] Institute for Molecular Science, National Institutes of Natural Sciences, Myodaiji, Okazaki 444-8585, Japan

First published on: 09 September 2010

To cite this Article Ohshima, Yasuhiro and Hasegawa, Hirokazu(2010) 'Coherent rotational excitation by intense nonresonant laser fields', International Reviews in Physical Chemistry, 29: 4, 619 — 663, First published on: 09 September 2010 (iFirst)
To link to this Article: DOI: 10.1080/0144235X.2010.511769
URL: http://dx.doi.org/10.1080/0144235X.2010.511769

International Reviews in Physical Chemistry
Vol. 29, No. 4, October–December 2010, 619–663

Taylor & Francis
Taylor & Francis Group

Coherent rotational excitation by intense nonresonant laser fields

Yasuhiro Ohshima* and Hirokazu Hasegawa

Institute for Molecular Science, National Institutes of Natural Sciences, Myodaiji, Okazaki 444-8585, Japan; The Graduate University for Advanced Studies, Myodaiji, Okazaki 444-8585, Japan

(*Received 14 June 2010; final version received 6 July 2010*)

The rotation of molecules in the gas phase can be coherently excited by irradiation with strong nonresonant short laser pulses, interacting with the molecular anisotropic polarisability. Such coherent rotational excitation has been attracting much attention because of the intriguing nature of the rotational wave packet thus created, and its wide applicability to dynamical studies and advanced optics. In this review article, we first survey various experimental schemes adopted so far for externally controlling molecular rotation, and then describe a new approach based on a quantum-state resolved spectroscopic probe for investigating coherent rotational excitation by intense nonresonant laser fields. Representative examples are given to show how the method provides detailed information on excitation pathways in wave-packet creation, and how it realises full quantum-state reconstruction of the rotational wave packet in a favourable case. We also describe an advanced wave-packet control, i.e. the creation and characterisation of a unidirectionally rotating wave packet, and discuss a further extension of this approach to explore coherent vibrational excitation.

Keywords: intense laser physics; molecular alignment; quantum-state distribution; rotational wave packet; angular-momentum orientation

Contents

*Corresponding author. Email: ohshima@ims.ac.jp

ISSN 0144–235X print/ISSN 1366–591X online

DOI: 10.1080/0144235X.2010.511769
http://www.informaworld.com

1. Introduction

Gas-phase molecules in an ordinary thermal condition undergo translational, rotational and vibrational motions in a random manner, and the total molecular system is a statistical ensemble that contains a number of molecules in many different states of motion. Manipulating such microscopic states of motion of atoms and molecules has been a great challenge in physics and chemistry. One of the greatest accomplishments in this direction is ultracold quantum degenerate states pertinent to the translational motion of atoms, now widely known as Bose–Einstein condensates (BECs); the experimental realisation was awarded a Nobel Prize in Physics in 2001 [1]. Since then, BECs have become an indispensable playground to test the basic concepts in various fields of physics [2]. Translationally cold molecules have recently emerged as the next fascinating target, and extensive studies have been devoted to creating them for use in fundamental physics and novel chemistry under ultracold conditions. The present status in this field is described in recent review articles [3,4].

In addition to translation, other degrees of freedom have been subjected to intensive studies pursuing the manipulation of molecular motions. In particular, control over rotation is of significance in elucidating structural information and the chemical reactivity of molecules [5]. Since these molecular properties have a strong dependence on the orientation of molecules in space, many important features are smeared out by averaging over the angular degrees of freedom for isotropic ensembles. If anisotropy is introduced in the system, the information that we can extract becomes much richer. Such a situation is paralleled in X-ray crystallography, where precise structural determinations of complex biomolecules are feasible from 3-D diffraction patterns of well-ordered crystals, but only radial information can be obtained from Debye–Scherrer patterns of powder samples composed of randomly oriented microcrystals.

To date, various approaches have been proposed and demonstrated to produce anisotropic distributions in gas-phase molecular ensembles. Among them, a few studies have reported experiments utilising directional inelastic collisions [6], particularly in supersonic expansions [7]. Other investigations rely on the exertion of external fields. They include the utilisation of inhomogeneous electric fields for state selection and subsequent focusing [8], the application of high electrostatic fields to trap freely rotating molecules in oriented states [9–11] and the implementation of polarised radiation resonant with optical transitions [12,13]. In addition to these, the exploitation of nonresonant intense laser pulses has been increasing dramatically [14,15], stimulated by recent rapid advances in

laser technologies. When gaseous molecules are exposed to an intense nonresonant laser field, a torque is exerted so as to align the molecular axis along the laser polarisation vector due to the interaction between the laser field and the molecular anisotropic polarisability. If the laser pulse duration is much shorter than the molecular rotational period, the irradiated molecular ensemble remains in a nonstationary quantum state of motion, even after the laser field is diminished. Accordingly, the angular distribution pertinent to the molecular orientation exhibits complex spatiotemporal propagation and, in most cases, shows characteristic recurrences (rotational revivals), at which the molecules are periodically aligned, with a specific time duration related to the molecular moments of inertia [16–18]. This situation is illustrated in Figure 1. The process, now commonly termed 'nonadiabatic molecular alignment', has been attracting much attention because of the interesting physics involved [14,15]. Many studies of the time-dependent spatial distribution of molecular ensembles have been reported, implementing various probing methods, e.g. Coulomb explosion imaging [19–21], photofragment imaging [22–25], high-order harmonic generation [26], instantaneous birefringence [27] and degenerate four-wave mixing [28,29]. Nonadiabatic molecular alignment has also been applied in many studies, in which the field-free molecular alignment in the space-fixed frame is extensively exploited to extract anisotropic molecular properties represented in the molecular-fixed frame [30–50].

The nonstationary quantum state, i.e. rotational wave packet, created in nonadiabatic molecular alignment is a coherent superposition of eigenstates, in which the rotational angular momentum J ranges among various values while its projection onto the space-fixed axis, M, is preserved at its initial values. Thus, nonadiabatic alignment is inherently accomplished by nonadiabatic rotational excitation (NAREX). Recently, the authors' research group and others have reported experimental studies conducted by utilising a frequency-domain spectroscopic probe on the rotational distribution after NAREX with almost full quantum-state resolution [51–57]. It has been shown that such a state-resolved investigation can afford details concerning the excitation process during exposure to laser

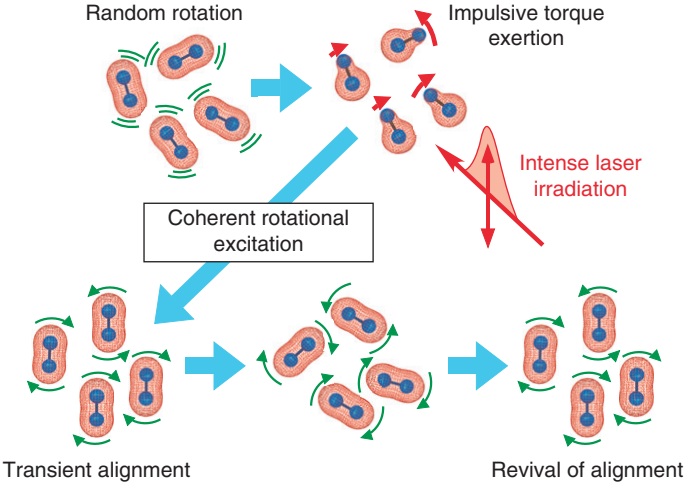

Figure 1. [Colour online] Illustration for nonadiabatic molecular alignment.

fields and, in a favourable case, full characterisation of a rotational wave packet itself. In addition, frequency-domain investigations can directly assess ultrafast control of the rotational-state distribution *via* the manipulation of rotational wave packets [52,58–61]. In this respect, the new approach based on quantum-state-resolved measurements is complementary to the aforementioned well-established methods, mostly probing the degree of alignment, and is thus a promising tool for exploring the underlying physics and developing novel applications in the evolutionally expanding field of nonadiabatic molecular alignment or NAREX. This article attempts to provide an overview of the research so far conducted in this field, focusing on selected topics to examine the utility of the newly developed approach.

This article is organised as follows. In Section 2, we summarise preceding studies concerning external control over molecular rotation based on various approaches, while emphasising developments with intense nonresonant laser pulses. Section 3 describes the basic theory needed to discuss nonadiabatic molecular alignment/NAREX *via* interactions with nonresonant radiation fields. In Section 4, we address some experimental details of the state-selective approach recently introduced in studies of NAREX. In Section 5, several examples are presented to show the utility of measurements on the rotational-state distribution. Finally, we remark on the outlook and make conclusions in Section 6.

2. Approaches to control of molecular rotation

2.1. *Orientation by electrostatic field*

When a static electric field is applied to a polar molecule, each rotational level, degenerate in the absence of a field, is split by the Stark effect into sublevels with different values of $|M|$. If an inhomogeneous field is applied by implementing, e.g. a hexapole, each of the sublevels feels different forces due to the $|M|$-dependent interaction, and thus an anisotropic subset can be selected from the total ensemble. Such state-focusing and filtering methods, well established more than two decades ago [8], are still being actively utilised in studies of photodissociation [62], bimolecular reactions [63] and molecular structure [64].

If the field strength is large enough, field-free rotational quantum states with different J values are mixed by the dipole–field interaction to form new eigenstates. The interaction potential has a deep minimum when the molecular dipole points along the applied electric field, and low-lying eigenstates have large probability in this direction. Thus, the molecular dipole (and consequently the molecular-fixed axis) is on average 'oriented' with respect to the space-fixed axis. This is similar to a pendulum in a gravitational field; so it is commonly termed a 'pendular state' [9]. This 'brute force' orientation [10] of molecular ensembles in the laboratory frame has also been adopted for examining steric effects in reactive collisions [11] and directional photodissociation dynamics [65–67], as well as various spectroscopic applications [68–70] (see also [15,71]). A number of theoretical studies have also been reported concerning the evolution of the 'pendular state' and related dynamics, as cited in [72]. In most of the experiments reported so far, the initial molecular ensemble is prepared in an adiabatic expansion to concentrate the population in low-energy rotational levels. Since the molecules travel from the field-free region into the electrostatic field, the dipole–field interaction is, strictly speaking, time dependent. However, the travelling time (in the ~μs regime) is so much slower than the molecular

rotational period (typically in the ~ps regime) that the interaction can be regarded as varying adiabatically in most cases, although nonadiabaticity may play a role in some cases, particularly for asymmetric-top molecules [73,74].

2.2. *Alignment and orientation by resonant transitions*

Interactions with radiation fields also produce an anisotropic molecular ensemble. It is well known that optical transitions by polarised radiation create an inhomogeneous M-sublevel distribution in the final state *via* the interaction with the molecular transition dipole [12,75,76]. A highly anisotropic distribution has been achieved by optical pumping, by the cycling of one-photon resonant excitation with polarised irradiation, followed by spontaneous emission [13]. Two-photon resonant stimulated Raman pumping has also been used frequently to generate anisotropic ensembles [77]. All-optical selection of M sublevels has been demonstrated by employing Autler–Townes splitting induced by resonant electronic transitions [78,79]. It is noted that the anisotropy induced herein is restricted to a subset with limited values of J, since all of the methods rely on resonant transitions. The resultant states after irradiation are those with 'aligned' or 'oriented' rotational angular momenta for linear or circular polarisation, respectively. Here, the populations in the former case are the same for $\pm M$; nevertheless, those for different $|M|$ differ from one another. The populations in the latter are different for $+M$ and $-M$. In both cases, the molecular-fixed axis is aligned, i.e. preferentially points parallel or perpendicular to the space-fixed axis, but there is no 'head-or-tail' distinction, as exhibited in electrostatic fields.

2.3. *Adiabatic alignment by nonresonant optical fields*

When the radiation is far off-resonant from any molecular transition, the field–matter interaction arises from the anisotropic polarisability [14,15], which is significant for most molecules. It contributes only in higher order than the dipole interaction, which depends linearly on the field strength. Nevertheless, by using modern advanced lasers, the optical interaction can overwhelm the static pendular potential. For instance, the static field is usually limited to ca. 10 MV/m by the occurrence of discharges between the electrodes, and the corresponding interaction is only $\sim 2\,\mathrm{cm}^{-1}$ for a dipole moment of 1 D ($\approx 3.336 \times 10^{-30}\,\mathrm{C\,m}$). The potential is so shallow that only low-lying states of heavy molecules can be trapped with substantial rotational cooling. On the contrary, there is no difficulty in achieving an optical field of 10 GV/m with commercially available pulsed lasers, partly owing to the good spatial coherence of laser fields. Taking $1\,\mathrm{\AA}^3$ ($\approx 1.1126 \times 10^{-40}\,\mathrm{C^2\,m^2/J}$) as a typical anisotropic polarisability, the interaction energy reaches $\sim 500\,\mathrm{cm}^{-1}$. This value is much larger than the energy intervals for the free rotation of lighter molecules, and the resultant molecular states exhibit a fairly high degree of anisotropy. This is the most attractive feature of the method with nonresonant radiation, even though it cannot easily achieve orientation of the molecular-fixed frame, as does the static pendular state. In addition, the whole molecular ensemble is subjected to the introduction of anisotropy, since the interaction is not related to any specific optical transitions.

Motivated by the above-mentioned advantages, the control of rotational motions by intense nonresonant laser fields has now emerged as a rapidly evolving field of research [14,15]. The manifestations of control can be categorised essentially into two types: one involves an adiabatic regime, and the other a nonadiabatic regime. The former corresponds to the situation where the field variation is much slower than the molecular rotational period. Experiments using nanosecond (ns)-pulsed lasers are of this type. Here, the system can be regarded as being in a stationary state governed by the interaction potential, which depends on time only parametrically. The problem is then formally the same as for strong static fields, except for a small difference in the functional form for the potentials. Such an 'optical pendular state' was initially proposed in 1995 [80,81], and soon after exemplified in stimulated Raman spectroscopic studies of molecular clusters [82,83], with band contours much different from field-free cases [84]. A direct verification of spatial alignment was achieved by using ion imaging of photofragments from optically aligned iodine molecules [85,86]. These studies showed that the degree of alignment follows in time the pulse envelope of the aligning ns laser. This is a clear manifestation of the adiabatic nature of the process, where the field-free levels are smoothly modified to the corresponding pendular states as the laser field rises, and then they gradually go back as the field diminishes to recover the original isotropic ensemble [14]. Since then, this 'adiabatic molecular alignment' has been utilised to control the photodissociation dynamics [87–89] and to determine the anisotropic polarisability of rare gas dimers [90]. In addition, the alignment associated with a structural deformation of CS_2 has been studied [91] and the degree of alignment has been directly assessed by pulsed gas electron diffraction [92,93].

In the aforementioned studies, using linearly polarised light, the molecular alignment is one-dimensional (1-D), with the major axis of the polarisability tensor aligned parallel to the laser polarisation. Circular polarisation also provides 1-D alignment, as described in the following section. However, the implementation of elliptically polarised light can afford 3-D alignment for asymmetric-top molecules [14,94], and this has already been demonstrated experimentally [95]. More sophisticated control over rotation in the adiabatic regime is the attainment of orientation by combining a moderate electrostatic field with a strong nonresonant laser field [96–98]. This control scenario was proposed in 1999 [96], and experimentally realised for polar linear molecules, OCS [99,100] and novel Xe-containing hydrides [101–103]. The 3-D orientation of an asymmetric-top molecule has also been reported by using electrostatic and elliptically polarised laser fields [104]. Quite recently, progress in the preparation of initial molecular ensembles has opened up a new possibility in adiabatic control. It has been shown that extensive rotational cooling down to <1 K provides a degree of alignment reaching to $\sim$0.9 [105]. Rotational-state selection by an inhomogeneous electrostatic deflector has been implemented to give an even better degree of alignment and substantial orientation [106–108]. The combination of two-colour phase-locked intense laser pulses has been proposed for all optical adiabatic orientations [109], and experimentally verified quite recently [110].

2.4. *Nonadiabatic alignment*

The initial demonstration of nonadiabatic alignment with off-resonant optical fields was achieved almost 40 years ago, by observing transient birefringence induced by

aligned molecules [111,112]. Slightly later, a closely related method, rotational coherence spectroscopy (RCS), was developed as a counterpart employing resonant transitions [113–115]. The rotational wave packet thus created was composed of eigenstates with J ranging among several values while M was preserved at the initial values (for the case of linear polarisation). All the early investigations were conducted in a weak-field regime, where the Rabi oscillation is so slow that the number of eigenstates involved is limited by a single-step one- or two-photon coupling with $\Delta J = \pm 1$ or ± 2. However, for a stronger field, much broader J values participate *via* multi-step coupling, and the resultant wave packet shows a much sharper angular distribution. This situation was first discussed thoroughly in 1995 [16]. Since then, many theoretical studies have predicted novel phenomena in strong-field nonadiabatic alignment, for instance, a post-pulse enhancement of alignment [17,18,116–118]. The first experimental verification was reported in 2001, where rotational revivals were clearly seen in the time-dependent angular distribution probed by ion imaging [19]. This has been followed by an explosion of studies on various molecular systems, e.g. diatomic [20,21,26,29,119–122], linear [27,28,123,124], symmetric-top [25] and asymmetric-top [22–24,125,126] molecules. In a closely related study, the creation of a rotational wave packet composed of multiple eigenstates was reported in a resonance Raman study with intense ultrafast pulses [127].

Studies on strong-field nonadiabatic alignment have been taking diverse directions. As a natural route to foster controllability, excitation with a pair of ultrafast pulses has been applied for a further enhancement of alignment [128,129]. Quite recently, repetitive impulsive excitation with eight pulses was reported to achieve high alignment in a room-temperature sample [130]. Double-pulse excitation has also been examined, particularly for applications to information processing [31,32,36], and for the selective alignment of isotopomers and spin isomers [37,38,131]. In addition, an orthogonally polarised pair has been shown to give a transient 3-D alignment of asymmetric-top molecules [132,133]. A combination of short ($\sim$0.1–1 ps) and long ($\sim$10 ns) pulses has been used for alignment enhancement [134] and 3-D alignment [135,136]. Excitation by elliptically polarised pulses has been studied for the characterisation and realisation of 3-D alignment [137,138]. Several advanced pulse-shaping technologies have also been implemented. They include adiabatic turn-on and sudden turn-off of the pulses [139,140], spectral phase modulation [141,142] and adaptive control [143–146]. Two oppositely chirped pulses have been shown to accelerate the molecular rotation to induce bond breakage by the centrifugal force [147–149]. The combination of a rapidly turned-off pulse with a static field has been proposed to achieve nonadiabatic orientation [150], and has been verified experimentally [151]. Quite recently, orientation has also been realised by two-colour phase-locked intense short pulses [152] and quantum-state selection, followed by impulsive excitation [153,154]. Single-shot imaging of transient alignment has been recorded by time-resolved optical polarigraphy [155]. Nonadiabatic molecular alignment has also been utilised extensively in many applications. They include an examination of the angular dependence pertinent to tunnelling ionisation dynamics [30,35,40,45,156,157], direct imaging of molecular orbitals and electron dynamics [33,34,39,43,48], mapping out the generation process of high harmonic generation (HHG) [158–161], advanced control of HHG, particularly related to attosecond pulse generation [41,42,44,46,50] and structural determinations [47,48].

3. Theoretical consideration on nonadiabatic rotational excitation

3.1. *Interaction terms*

The interaction with a radiation field is most properly approximated as that associated with the electric dipole moment of a molecule. When the radiation is far-off resonant from any molecular transitions, the semiclassical perturbative treatment, with which the field is regarded as a classical wave, while the molecular system is quantal, casts the interaction into a form that involves molecular polarisability as [15]

$$\widehat{V}(t) = -\frac{1}{2}\sum_{\alpha,\beta} \alpha_{\alpha\beta} E_\alpha(t) E_\beta(t), \tag{1}$$

where E_α is the space-fixed Cartesian component of the radiation field vector and $\alpha_{\alpha\beta}$ is that of the molecular polarisability tensor ($\alpha, \beta = X, Y, Z$). This equation can be simply explained in a phenomenological manner. When an external electronic field is applied, a dipole moment is induced due to a finite molecular polarisability as

$$(\mu_{\text{ind}})_\alpha = \sum_\beta \alpha_{\alpha\beta} E_\beta. \tag{2}$$

It is noted that the induced dipole may not be parallel to the applied field in an arbitrary case. After taking the integral of the induced dipole–field interaction, we have

$$\widehat{V}(t) = -\int \mu_{\text{ind}} \bullet dE = -\int \sum_{\alpha,\beta} \alpha_{\alpha\beta} E_\beta \, dE_\alpha = -\frac{1}{2}\sum_{\alpha,\beta} \alpha_{\alpha\beta} E_\alpha E_\beta. \tag{3}$$

It will be convenient to recast Equation (1) with a spherical tensor of rank k, $T^{(k)}(\alpha)$, since we can fully utilise the mechanical algebra of the spherical tensor formalism. We thus have

$$\widehat{V}(t) = -\frac{1}{2}\sum_{k=0}^{2} T^{(k)}(\alpha) \cdot T^{(k)}(E, E). \tag{4}$$

$T^{(k)}(E, E)$ is the tensor product of the electric field vectors [75], of which the component is

$$T_p^{(k)}(E, E) = \left[E^{(1)} \otimes E^{(1)}\right]_p^{(k)} = \sum_{p_1+p_2=p} E_{p_1}^{(1)} E_{p_2}^{(1)} \langle 1, p_1, 1, p_2 | k, p \rangle, \tag{5}$$

where $\langle \cdots | \cdots \rangle$ is the Clebsch–Gordan coefficient, and the field vectors are represented in the spherical tensor form as

$$E_0^{(1)} = E_Z, \quad E_{\pm 1}^{(1)} = \mp \frac{1}{\sqrt{2}} [E_X \pm i E_Y]. \tag{6}$$

We are now considering the far-off resonant case, so that the polarisability tensor is symmetric and those of odd rank vanish by symmetry, to recast Equation (4) as

$$\widehat{V}(t) = -\frac{1}{2} T_0^{(0)}(\alpha) T_0^{(0)}(E, E) - \frac{1}{2}\sum_{p=-2}^{2} (-1)^p T_p^{(2)}(\alpha) T_{-p}^{(2)}(E, E). \tag{7}$$

Next, we introduce the rotational matrix $D^{(k)}_{p,q}$ to transform the molecular properties represented in the space-fixed frame (for which index p is used) to those in the molecular-fixed frame (with index q) [75]:

$$\widehat{V}(t) = -\frac{1}{2} D^{(0)*}_{0,0} T^{(0)}_0(\alpha) T^{(0)}_0(E,E) - \frac{1}{2} \sum_{p=-2}^{2} \sum_{q=-2}^{2} (-1)^p D^{(2)*}_{p,q} T^{(2)}_q(\alpha) T^{(2)}_{-p}(E,E). \tag{8}$$

The molecular-fixed frame is commonly set to the principal axes for the molecular moment of inertia because of a much simpler treatment of the energy levels, especially in the field-free condition. Then, the nonzero tensor components of polarisability are given with the molecular-fixed Cartesian components as

$$\begin{aligned} T^{(0)}_0(\alpha) &= -\frac{1}{\sqrt{3}}\left[\alpha_{xx} + \alpha_{yy} + \alpha_{zz}\right], \quad & T^{(2)}_0(\alpha) &= \frac{1}{\sqrt{6}}\left[2\alpha_{zz} - \alpha_{yy} - \alpha_{xx}\right] \\ T^{(2)}_{\pm 1}(\alpha) &= \mp\left[\alpha_{xz} \pm i\alpha_{yz}\right], & T^{(2)}_{\pm 2}(\alpha) &= \frac{1}{2}\left[\left(\alpha_{xx} - \alpha_{yy}\right) \pm 2i\alpha_{xy}\right]. \end{aligned} \tag{9}$$

If the molecular shape is orthorhombic, the off-diagonal Cartesian components diminish, to yield three independent parameters, $T^{(0)}_0(\alpha)$, $T^{(2)}_0(\alpha)$ and $T^{(2)}_2(\alpha) = T^{(2)}_{-2}(\alpha)$. Symmetric-top or linear molecules possess the following two components only by symmetry:

$$T^{(0)}_0(\alpha) = -\frac{1}{\sqrt{3}}\left[\alpha_{\parallel} + 2\alpha_{\perp}\right] \equiv -\sqrt{3}\bar{\alpha}, \quad T^{(2)}_0(\alpha) = \frac{2}{\sqrt{6}}\left[\alpha_{\parallel} - \alpha_{\perp}\right] \equiv \frac{2}{\sqrt{6}}\Delta\alpha, \tag{10}$$

with $\alpha_{\parallel}$ and $\alpha_{\perp}$ for the parallel and perpendicular components to the molecular symmetry axis, respectively.

In a further treatment of Equation (8), there are several choices for the laser polarisation direction. First, we consider a linearly polarised field along the space-fixed Z-axis in the form of

$$\mathbf{E}(t) = {}^t\big(0, 0, \varepsilon(t)\cos(\omega t + \delta)\big) \equiv {}^t\big(0, 0, E(t)\big), \tag{11}$$

with $\varepsilon(t)$ being the pulse envelope, ω the carrier frequency and δ the phase offset. Since $T^{(0)}_0(E,E)$ and $T^{(2)}_0(E,E)$ are only nonvanishing, the interaction for orthorhombic molecules is represented as

$$\widehat{V}(t) = \left\{\frac{1}{2\sqrt{3}} T^{(0)}_0(\alpha) - \frac{1}{\sqrt{6}}\left[D^{(2)*}_{0,0} T^{(2)}_0(\alpha) + \left(D^{(2)*}_{0,2} + D^{(2)*}_{0,-2}\right) T^{(2)}_2(\alpha)\right]\right\}[E(t)]^2. \tag{12}$$

The interaction can be averaged over the optical cycles due to the off-resonant condition [15], to have

$$\widehat{V}(t) = \frac{1}{2}[\varepsilon(t)]^2\left\{\frac{1}{2\sqrt{3}} T^{(0)}_0(\alpha) - \frac{1}{\sqrt{6}}\left[D^{(2)*}_{0,0} T^{(2)}_0(\alpha) + \left(D^{(2)*}_{0,2} + D^{(2)*}_{0,-2}\right) T^{(2)}_2(\alpha)\right]\right\}. \tag{13}$$

Thus, it depends only on the pulse envelope, irrelevant of the carrier frequency and the phase. Equation (13) is recast by substituting the explicit forms for the rotational matrices [73] as

$$\widehat{V}(t) = -\frac{1}{4}[\varepsilon(t)]^2\left[\alpha_{xx} + (\alpha_{zz} - \alpha_{xx})\cos^2\theta + \left(\alpha_{yy} - \alpha_{xx}\right)\sin^2\theta\sin^2\chi\right], \tag{14}$$

where θ and χ represent the Euler angle between the molecular-fixed z-axis and the laser polarisation direction (i.e. space-fixed Z-axis), and that of rotation around the z-axis [15]. This expression is independent from the angle ϕ of rotation around the Z-axis, which is a clear signature of 1-D alignment by linear polarisation. For symmetric-top or linear molecules, the interaction is much simpler, given as

$$\widehat{V}(t) = -\frac{1}{12}[\varepsilon(t)]^2\left\{\left(\alpha_{\parallel} + 2\alpha_{\perp}\right) + 2D_{0,0}^{(2)*}\Delta\alpha\right\} = -\frac{1}{4}[\varepsilon(t)]^2\left(\alpha_{\perp} + \Delta\alpha\cos^2\theta\right). \tag{15}$$

This interaction forces the molecular axis to be aligned parallel to the Z-axis for $\Delta\alpha > 0$.

The space-fixed axes can be differently defined for the linear polarisation. Here, the Z-axis is set along the laser propagation direction and the polarisation vector pointing to the X-axis. This choice of the axes is convenient for the case when we implement multiple linearly polarised pulses with their polarisation vectors tilted to another, as discussed later. The field components are

$$\mathbf{E}(t) = {}^t\left(\varepsilon(t)\cos(\omega t + \delta), 0, 0\right) \equiv {}^t\left(E(t), 0, 0\right). \tag{16}$$

Then, the nonzero tensor products are

$$T_0^{(0)}(E,E) = -\frac{1}{\sqrt{3}}[E(t)]^2 = \sqrt{2}T_0^{(2)}(E,E) = -\frac{2}{\sqrt{3}}T_{\pm 2}^{(2)}(E,E). \tag{17}$$

In the case of orthorhombic molecules, the cycle-averaged interaction is represented as

$$\begin{aligned}\widehat{V}(t) = \frac{1}{4}[\varepsilon(t)]^2\Bigg\{&\frac{1}{\sqrt{3}}T_0^{(0)}(\alpha) + \left[\frac{1}{\sqrt{6}}D_{0,0}^{(2)*} - \frac{1}{2}\left(D_{2,0}^{(2)*} + D_{-2,0}^{(2)*}\right)\right]T_0^{(2)}(\alpha)\\ &+ \left[\frac{1}{\sqrt{6}}\left(D_{0,2}^{(2)*} + D_{0,-2}^{(2)*}\right) - \frac{1}{2}\left(D_{2,2}^{(2)*} + D_{2,-2}^{(2)*} + D_{-2,2}^{(2)*} + D_{-2,-2}^{(2)*}\right)\right]T_2^{(2)}(\alpha)\Bigg\}.\end{aligned} \tag{18}$$

For symmetric-top or linear molecules, it can be given as

$$\begin{aligned}\widehat{V}(t) &= -\frac{1}{12}[\varepsilon(t)]^2\left\{\left(\alpha_{\parallel} + 2\alpha_{\perp}\right) - \Delta\alpha D_{0,0}^{(2)*} + \sqrt{\frac{3}{2}}\Delta\alpha\left[D_{-2,0}^{(2)*} + D_{2,0}^{(2)*}\right]\right\}\\ &= \frac{1}{8}[\varepsilon(t)]^2\left\{\Delta\alpha[1 + \cos(2\phi)]\cos^2\theta - \Delta\alpha\cos(2\phi) - \left(\alpha_{\parallel} + \alpha_{\perp}\right)\right\}.\end{aligned} \tag{19}$$

As is expected, the interaction exerts a force to align the molecular axis perpendicular to the Z-axis at $\phi = 0$ or π for $\Delta\alpha > 0$.

When circular polarisation is implemented, the field components are denoted as

$$\mathbf{E}(t) = {}^t\left(\varepsilon(t)\cos(\omega t + \delta), \pm\varepsilon(t)\sin(\omega t + \delta), 0\right), \tag{20}$$

where the + and − signs correspond to right and left circular polarisation, respectively (with definition of [76]), and the laser propagation direction is set along the Z-axis. Then, the nonzero tensor products for the right circularity are

$$\begin{aligned}T_0^{(0)}(E,E) &= -\frac{1}{\sqrt{3}}\left[E_X^2 + E_Y^2\right] = -\frac{1}{\sqrt{3}}[\varepsilon(t)]^2 = \sqrt{2}T_0^{(2)}(E,E),\\ T_{\pm 2}^{(2)}(E,E) &= \frac{1}{2}\left[E_X^2 - E_Y^2 \pm 2iE_XE_Y\right] = \frac{1}{2}[\varepsilon(t)]^2\exp[\pm 2i(\omega t + \delta)].\end{aligned} \tag{21}$$

Since the interaction is a linear combination of the tensor products, we take their optical cycle averages as

$$T_0^{(0)}(E,E) \to -\frac{1}{\sqrt{3}}[\varepsilon(t)]^2 = \sqrt{2}T_0^{(2)}(E,E), \quad T_{\pm 2}^{(2)}(E,E) \to 0. \tag{22}$$

These values are the same for the left-circular polarisations. Then, the interaction for orthorhombic molecules is represented for both circularities as

$$\begin{aligned}\widehat{V}(t) &= \frac{1}{2}[\varepsilon(t)]^2\left\{\frac{1}{\sqrt{3}}T_0^{(0)}(\alpha) + \frac{1}{\sqrt{6}}D_{0,0}^{(2)*}T_0^{(2)}(\alpha) + \frac{1}{\sqrt{6}}\left(D_{0,2}^{(2)*} + D_{0,-2}^{(2)*}\right)T_2^{(2)}(\alpha)\right\} \\ &= -\frac{1}{4}[\varepsilon(t)]^2\left\{\left(\alpha_{zz}+\alpha_{yy}\right) - \left(\alpha_{zz}-\alpha_{xx}\right)\cos^2\theta + \left(\alpha_{xx}-\alpha_{yy}\right)\sin^2\theta\sin^2\chi\right\}. \end{aligned} \tag{23}$$

This expression is reduced into the following form for symmetric-top or linear molecules:

$$\widehat{V}(t) = -\frac{1}{6}[\varepsilon(t)]^2\left\{\left(\alpha_{\parallel}+2\alpha_{\perp}\right) - \left(\alpha_{\parallel}-\alpha_{\perp}\right)D_{0,0}^{(2)*}\right\} = -\frac{1}{4}[\varepsilon(t)]^2\left\{\left(\Delta\alpha + 2\alpha_{\perp}\right) - \Delta\alpha\cos^2\theta\right\}. \tag{24}$$

This looks similar to Equation (15), but the molecular axis is forced to align perpendicular to the Z-axis for $\Delta\alpha > 0$ in this case. A more general consideration including elliptically polarised irradiation has been described in [94].

3.2. *Time evolution of rotational states*

Once the interaction with a radiation field is specified, the time evolution of the molecular states can be tracked. We assume here that molecules reside in stationary states before interacting with laser pulses. It is also assumed that the molecular Hamiltonian, $\hat{H}_0$, in the field-free condition and the corresponding rotational eigenstates are well characterised.

$$\hat{H}_0|r\rangle = E_r|r\rangle, \tag{25}$$

where r stands for an index to identify the eigenstates. For instance, when we consider a closed-shell symmetry-top molecule, like benzene, in which the electronic orbital and the spin angular momenta are quenched, the eigenstates are represented with a rotational matrix as

$$|r\rangle = |J,K,M\rangle = \sqrt{\frac{2J+1}{8\pi^2}}D_{M,K}^{(J)*}(\phi,\theta,\chi), \tag{26}$$

with K being the projection of J onto the molecular symmetry axis. The eigen energy for $|J,K,M\rangle$ is

$$E_r = E_{J,K} = hcBJ(J+1) + hc(C-B)K^2, \tag{27}$$

where B and C are rotational constants (in cm^{-1} unit) with respect to the b- and c-axes (the latter being the figure axis), and h and c are the Planck constant and the speed of light. Centrifugal-distortion terms are not included in Equation (28) for simplicity (their contribution may be negligible in the range of J to be considered).

In many cases, the initial ensemble is a mixture of molecules in many different eigenstates, but we first take a single rotational level as an initial state, $|r_i\rangle$. The nonadiabatic interaction with the nonresonant ultrafast laser field converts the stationary state to a rotational wave packet, $\left|\Psi(t)\right\rangle$, which is expanded as

$$\left|\Psi_{r_i}(t)\right\rangle = \hat{U}(t,0)|r_i\rangle = \sum_r C_{r_i,r}\exp(-i\omega_r t)|r\rangle. \tag{28}$$

Here, $\hat{U}(t_2,t_1)$ is the time-evolution operator from time t_1 to t_2 and $\omega_r = E_r/\hbar$. The complex expansion coefficient appearing in Equation (28) is factored as

$$C_{r_i,r} = A_{r_i,r}\exp\left(i\delta_{r_i,r}\right), \tag{29}$$

where $A_{r_i,r}$ and $\delta_{r_i,r}$ are the amplitude and the phase of each $|r\rangle$ state, respectively. Both of them have real values. Because the time evolution maintains microscopic equilibrium, the coefficient $C_{r',r}$ is identical to $C_{r,r'}$, giving

$$A_{r',r} = A_{r,r'}, \quad \delta_{r',r} = \delta_{r,r'}. \tag{30}$$

These identities have been numerically validated. These expansion coefficients vary during the interaction with the laser pulses. They subsequently become constant after the laser field vanishes, and the time propagation of the wave packet is entirely described with the $\exp(-i\omega_r t)$ terms, depending on the field-free energies. Exact values of the amplitudes and phases in the rotational wave packet can be derived by solving the time-dependent Schrödinger equation (TDSE) with the initial condition, $\left|\Psi(t\to-\infty)\right\rangle = |r_i\rangle$,

$$i\hbar\frac{\partial}{\partial t}\left|\Psi_{r_i}(t)\right\rangle = \left[\hat{H}_0 + \hat{V}(t)\right]\left|\Psi_{r_i}(t)\right\rangle. \tag{31}$$

Substituting Equation (28), this TDSE is recast into the following coupled differential equations for the expansion coefficients:

$$i\hbar\frac{d}{dt}C_{r_i,r}(t) = \sum_{r'}\langle r|\hat{V}(t)|r'\rangle\exp\left(-i\Delta\omega_{r',r}t\right)C_{r_i,r'}(t), \tag{32}$$

where $\Delta\omega_{r',r} = \omega_{r'} - \omega_r$. These coupled equations can be solved numerically to determine the complex expansion coefficients, once $\hat{V}(t)$ is specified. The interaction is expanded with rotational matrices, as shown in the preceding section, and the evaluation of its matrix elements is straightforward when we adopt a symmetric-top basis set, using general formula for the rotational matrix, as

$$\begin{aligned}&\left\langle J',K',M'\right|D^{(2)*}_{p,q}|J,K,M\rangle \\ &\quad = (-1)^{M'-K'}\sqrt{(2J'+1)(2J+1)}\begin{pmatrix} J' & 2 & J \\ -K' & q & K\end{pmatrix}\begin{pmatrix} J' & 2 & J \\ -M' & p & M\end{pmatrix},\end{aligned} \tag{33}$$

where the round bracket denotes the Wigner's 3-j symbol. For instance, when a linearly polarised field along the space-fixed Z-axis is employed for NARAX, the interaction for symmetric-top molecules, denoted in Equation (15), has matrix elements only diagonal in K and M. Furthermore, they are nonvanishing only if $\Delta J = 0, \pm2$, for $K = 0$ and/or $M = 0$, or $\Delta J = 0, \pm1, \pm2$ for $K \neq 0$ and $M \neq 0$. It is also noted that states with the same parity are only coupled since the polarisability tensor is symmetric to the space inversion operation.

In this case, the K and M values in Equation (28) [where r represents a set of (J, K, M)] are preserved, while J can range among a wider distribution.

If molecules are distributed in different eigenstates in initial condition, we have to deal with an incoherent ensemble, which is described with the following density matrix:

$$\boldsymbol{\rho} = \sum_{r_i} W_{r_i} \left|\Psi_{r_i}(t)\right\rangle\left\langle\Psi_{r_i}(t)\right|, \tag{34}$$

where W_{r_i} stands for the initial population for state $|r_i\rangle$. The expectation value of a given observable, $\hat{A}$, can be obtained as

$$\left\langle\left\langle \hat{A} \right\rangle\right\rangle \equiv Tr\left(\boldsymbol{\rho}\hat{A}\right). \tag{35}$$

For instance, let us consider the expectation value of $\cos^2\theta$, which is frequently referred as a measure of the degree of alignment [15]. By adopting Equations (34) and (35), we have:

$$\begin{aligned}\left\langle\left\langle \cos^2\theta \right\rangle\right\rangle &= \sum_{r_i} W_{r_i}\left\langle\Psi_{r_i}(t)\right| \cos^2\theta \left|\Psi_{r_i}(t)\right\rangle \\ &= \sum_{r_i} W_{r_i} \sum_{r,r'} C^*_{r_i,r'} C_{r_i,r}\left\langle r'\right| \cos^2\theta |r\rangle \exp\left(i\Delta\omega_{r',r}t\right).\end{aligned} \tag{36}$$

As can be clearly seen, even after the laser field diminishes, it shows an oscillatory variation in time, of which the beat frequencies are proportional to the energy-level intervals. Since $\cos^2\theta$ is given as $D^{(2)*}_{0,0}$, its matrix element is evaluated by using Equation (33) for the case of symmetric-top molecules. Then, beat frequencies with $\Delta J = \pm 1, \pm 2$ only appear. Another example is the state distribution after the laser pulse, which can be probed by a state-selective examination. The population for each probed state $|r\rangle$ is given as

$$P_r \equiv \sum_{r_i} W_{r_i}\left|C_{r_i,r}\right|^2 = \sum_{r_i} W_{r_i}\left(A_{r_i,r}\right)^2, \tag{37}$$

so that the information on the composition of the wave packet is encoded.

We next consider the case when multiple pulses are employed to nonadiabatic excitation. If another laser pulse is irradiated onto the molecule at $t = \tau$, the wave packet created by the first pulse represented in Equation (28) is further modified by the interaction with the second pulse. The resultant wave packet at t after the second pulse is expanded as

$$\left|\Psi_{r_i}(t)\right\rangle = \hat{U}'(t,\tau)\left|\Psi_{r_i}(\tau)\right\rangle = \sum_r B_{r_i,r}(\tau)\exp(-i\omega_r t)|r\rangle, \tag{38}$$

where $B_{r_i,r}$ is the transition amplitude from the initial $|r_i\rangle$ state to $|r\rangle$ by the interaction with the double pulses, and represented by

$$B_{r_i,r}(\tau) = \sum_{r'} C_{r_i,r'} C'_{r',r} \exp\left(-i\Delta\omega_{r',r}\tau\right) = \sum_{r'} A_{r_i,r'} A'_{r',r} \exp\left[-i\left(\Delta\omega_{r',r}\tau - \delta_{r_i,r'} - \delta'_{r',r}\right)\right], \tag{39}$$

where the prime on the $C_{r_i,r}$ and $A_{r_i,r}$ coefficients indicates the properties by the second pulse. Equations (38) and (39) show that the wave packet after the interaction with two

successive short pulses can be fully described for an arbitral time delay between them once the amplitudes and phases of the constituent eigenstates in the wave packets created by each single pulse are known.

The simplest (but not uninteresting) application of the double-pulse excitation is that by using a pair of pulses with identical intensity and envelope, between which the delay is varied. The population of the rotational eigenstate, $|r\rangle$, after the interaction with such a pulse pair is the square of the absolute amplitudes given in Equation (39),

$$\left|B_{r_i,r}(\tau)\right|^2 = \sum_{r'} \left(A_{r_i,r'}\right)^2 \left(A_{r',r}\right)^2 + 2 \sum_{r' > r''} A_{r_i,r'} A_{r',r} A_{r_i,r''} A_{r'',r} \cos\left(\Delta\omega_{r',r''}\tau + \Delta_{r_i,r}^{r',r''}\right), \quad (40)$$

with

$$\Delta_{r_i,r}^{r',r''} = \delta_{r_i,r''} + \delta_{r'',r} - \delta_{r_i,r'} - \delta_{r',r}. \quad (41)$$

Equation (40) shows that the information on the phase and amplitude of each eigenstate constituting the rotational wave packet can be extracted from the delay-dependent population for the rotational levels after an interaction with the double-pulse pair. An experimental demonstration is described in Section 5.

The treatments of a linear molecule are quite similar to the procedure mentioned above. For a closed-shell molecule, the eigenstate in a field-free condition is represented as a spherical harmonics, $|J, M\rangle$, and the corresponding eigen energy and matrix elements are derived by simply disregarding the K quantum number, i.e. setting $K = 0$. For asymmetric-top molecules, each field-free eigenstate is represented as a linear combination of the symmetric-top wave functions as

$$|r\rangle = |J, \tau, M\rangle = \sum_K a_{\tau,K} |J, K, M\rangle, \quad (42)$$

where τ is an index for level ordering [75]. Thus, an evaluation of the interaction with the laser field is straightforward, yet somewhat laborious, by using matrix elements for the symmetric-top basis represented in Equation (33).

In the case of open-shell systems (here we only mention linear molecules), the electronic orbital and/or spin angular momenta, denoted by **L** and **S**, respectively, couple with the rotational angular momentum. There are two limiting representations to describe the angular-momentum coupling. In Hund's case (a), **L** and **S** are tied to the molecule so strongly that only their projections on the molecular axis, Λ and Σ, respectively, are preserved. Then, each rotational state is represented by using a basis set, $|J, \Omega, M\rangle$, with **J** being the angular momentum including the electron motion and Ω for its projection onto the molecular axis ($=\Lambda + \Sigma$) [75]. In this case, K appearing in Equation (33) should be replaced by Ω. The other is Hund's case (b), which is commonly adopted to molecules with $\mathbf{L} = 0$. Here, **S** couples to the rotational angular momentum **N** (instead of **J** used before for closed-shell molecules) to have the total angular momentum $\mathbf{J} = \mathbf{N} + \mathbf{S}$. Then, the rotational state is represented by a coupled basis set,

$$|N, S, J, M\rangle = \sum_{M_S + M_N = M} \langle N, M_N, S, M_S \mid J, M\rangle |N, M_N\rangle |S, M_S\rangle. \quad (43)$$

By using the basis functions, the matrix element of the rotational matrices to evaluate the interaction by the laser field is given as

$$\begin{aligned}
&\langle N', S, J', M' | D^{(2)*}_{p,0} | N, S, J, M\rangle \\
&\quad = (-1)^{J'-M'} \langle N', S, J' \| D^{(2)*}_{\cdot,0} \| N, S, J\rangle \begin{pmatrix} J' & 2 & J \\ -M' & p & M \end{pmatrix} \\
&\quad = (-1)^{J'-M'} \begin{pmatrix} J' & 2 & J \\ -M' & p & M \end{pmatrix} \\
&\qquad \times (-1)^{N'+S+J+2} \langle N' \| D^{(2)*}_{\cdot,0} \| N\rangle \sqrt{(2J'+1)(2J+1)} \begin{Bmatrix} N' & J' & S \\ J & N & 2 \end{Bmatrix} \\
&\quad = (-1)^{J'+J+2N'+S+2-M'} \sqrt{(2N'+1)(2N+1)(2J'+1)(2J+1)} \\
&\qquad \times \begin{Bmatrix} N' & J' & S \\ J & N & 2 \end{Bmatrix} \begin{pmatrix} N' & 2 & N \\ 0 & 0 & 0 \end{pmatrix} \begin{pmatrix} J' & 2 & J \\ -M' & p & M \end{pmatrix},
\end{aligned} \tag{44}$$

by employing the Wigner–Eckart theorem, where $\{\cdots\}$ is the Wigner's 6-j symbol and $\langle \| \| \rangle$ represents the reduced matrix element [75].

4. Experimental method

The experimental approach recently applied in an investigation on NAREX is based on the familiar pump–probe strategy. The schematic diagram for the experiments is shown in Figure 2. At the beginning, the molecular ensemble to be examined is adiabatically cooled in a supersonic expansion to concentrate the population to a narrow range of low-energy rotational levels. Next, intense nonresonant pulses with durations of femotosecond (fs) to picosecond (ps) regime are irradiated onto the molecules to induce NAREX in the vibronic ground state. Finally, the rotational-state distribution after the interaction with the ultrafast pulses is probed by the frequency-resolved spectroscopic method with ns pulses, i.e. resonance-enhanced multi-photon ionisation (REMPI). Though a vast number of pump–probe experiments have been reported so far, such a kind of totally different time scales in the pump and probe processes have been rarely adopted, except for precise coherent control by vibrational wave-packet interferometry [162,163]. Apart from the single difference, this approach deserves several inherent advantages (and some drawbacks also) much the same as the conventional pump–probe methods. For instance, like many studies in the ns regime, it benefits from duplex selection by mass analysis and resonant transitions owing to the REMPI probe employed. Thus, the effects by the intense ultrafast pulses are explored both in species- and state-specific manners. In addition, when we implement a pair of fs pump pulses with variable delay between them, the evolution of coherently created states is traced in real time, as is the case for well-established ultrafast pump–probe methods. On the other hand, it is necessary for molecules to be examined to have bound–bound transitions in the visible or near UV region suitable for a REMPI probe. This method is most closely related to ionisation-detected stimulated Raman spectroscopy (IDSRS) [164,165], particularly nonlinear Fourier-transform Raman spectroscopy using broadband ns pulses [166,167]. This method and IDSRS rely on the

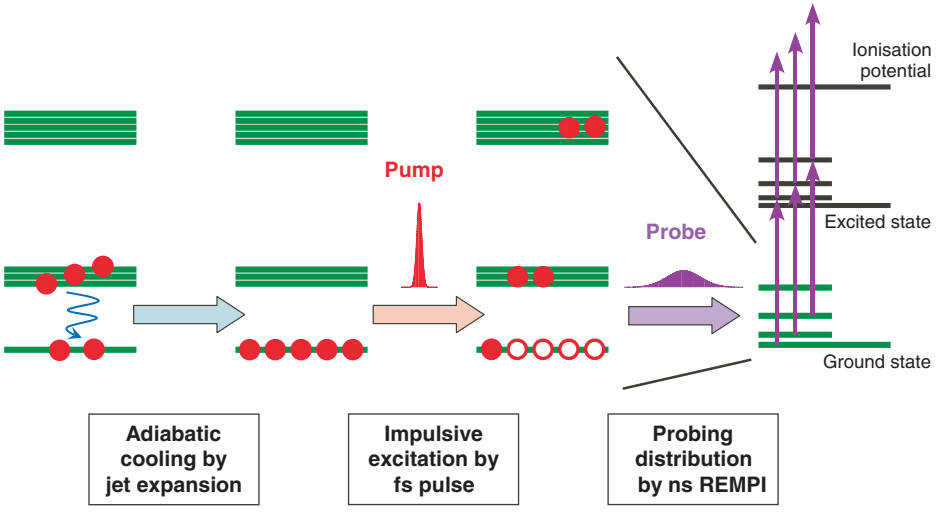

Figure 2. [Colour online] Experimental scheme for state-selective examination of nonadiabatic rotational excitation.

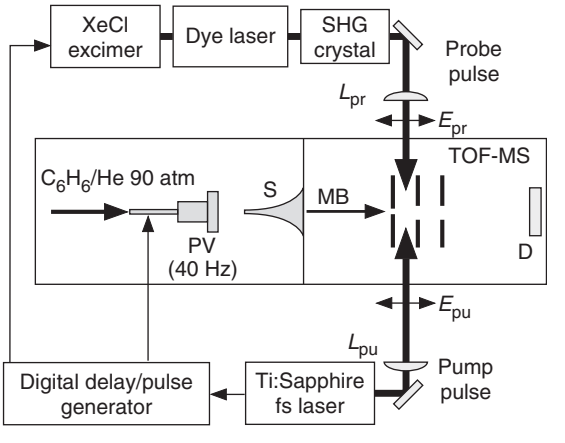

Figure 3. Schematic diagram of the experimental setup for state-selective examination of nonadiabatic rotational excitation. PV, pulsed valve; S, skimmer; MB, molecular beam; L_{pr}, lens for probe pulses; L_{pu}, lens for pump pulses; and D, MCP detector. E_{pu} and E_{pr} are the polarisation directions of the pump and probe pulses, respectively. From Ref. [53].

interaction of the molecular polarisability with nonresonant intense pulses, though their time scales (fs vs. ns) are much different from each other.

A typical experimental setup is schematically shown in Figure 3. It consists of three essential parts: a molecular beam chamber with a time-of-flight mass spectrometer (TOF-MS), an ultrafast laser system to deriver the pump pulses and a frequency-tunable ns laser system to conduct the state-specific probe. The first part may not be so specially designed. A mass resolution of $M/\Delta M \approx 300$ at $M \approx 100$ is sufficient for this purpose,

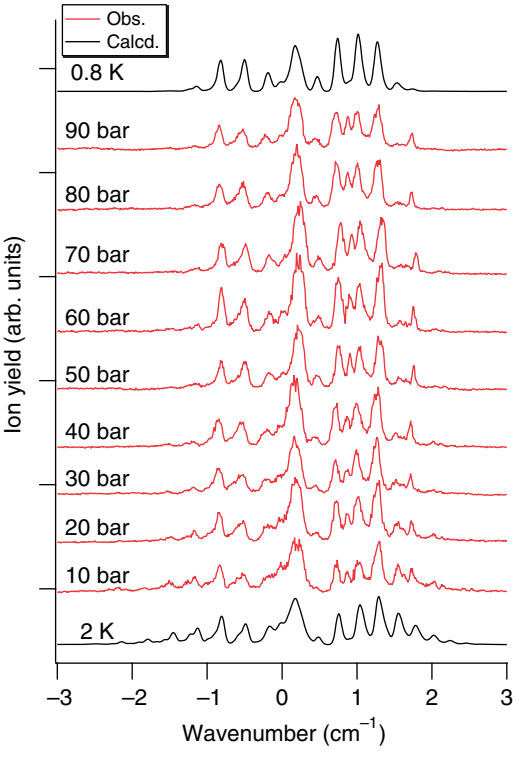

Figure 4. [Colour online] Stagnation pressure dependence of the (1 + 1) REMPI excitation spectrum of the $S_1 \leftarrow S_0\ 6_0^1$ band of benzene in a molecular beam with Ne as a buffer gas. Horizontal scale is indicated as a relative wave number from the band origin. Simulated spectra for 0.8 and 2 K are also indicated for comparison.

and it can be achieved without much difficulty by a linear TOF-MS with a relatively short (e.g. 50 cm long) flight region. In addition, pulsed molecular beams cooperate in most cases and thus the chamber should simply consist of beam-source, interaction and TOF/detection regions. An important issue for the beam source is the preparation of molecular ensembles with the rotational temperature being as low as possible. Since NAREX provides a broad distribution up to higher rotational levels, even from a single initial state, a restriction of initial states is crucial for a clear examination of the results after NAREX, particularly for moderately large molecules giving congested spectra, even at *ca* 10 K. In previous investigations by laser-induced fluorescence, intensive rotational cooling (<1 K) has been realised in a free-jet expansion with a modest stagnation pressure (up to 10 bar) [168–170]. On the other hand, there had been scarcely reported REMPI studies under such an extensive cooling condition, probably due to warming up of the jet steam by turbulence at the skimmer. A recently developed solenoid value has altered the situation very much [171]. It can produce narrow packets of molecular streams (<10 μs duration), even when operated at 90 bar. Consequently, the skimmer turbulence has been suppressed and efficient cooling has been attained. A typical performance of the high-pressure valve is shown in Figure 4. Here, we have examined the excitation spectrum of the $S_1 \leftarrow S_0\ 6_0^1$

vibronic band of normal benzene (C_6H_6), by varying the stagnation pressure from 10 to 90 bar. The number of the observed rotational lines is so limited and, in particular, there appear transitions only from $(J, K) = (0, 0)$, $(1, 0)$, $(1, 1)$, $(2, 2)$ and $(3, 3)$ for >50 bar. The observed spectrum is reasonably reproduced by that simulated at 0.8 K. Such a sub-K initial condition is certainly beneficial as detailed in the next section. It has to be pointed out that Q- and ^{p}R-branches are observed to be stronger than the simulation. The observed spectrum showed no change when we varied the polarisation direction of the linearly polarised excitation pulse parallel or perpendicular to the molecular-beam propagation direction. This observation has ruled out the possibility of any collisional alignment in the molecular beams [7]. We speculate that the discrepancy may come from the angular dependence of the ionisation efficiency, which appears *via* an alignment in the S_1 manifold imposed by the polarised excitation in a rotational-state dependent manner. Further studies are necessary for any definitive discussion.

To realise an appreciable NAREX in molecules with moderate polarisability, a laser pulse strength on the order of 1 J/cm^2 is necessary. This requirement has been fulfilled by employing ultrafast laser systems now commercially available. For instance, a multipass amplifier seeded with a mode-looked fs Ti:sapphire laser, installed in the authors' research group, provides near-infrared (centred at ~820 nm) pulses with up to 2.5 mJ/pulse and ~40 fs duration at 1 kHz. The output from the laser system is sent to cross the molecular beam in the orthogonal direction. In double-pulse excitation studies, the pump beam is split into two pulses of equal intensity in a Michelson interferometer, and one of them is appropriately delayed against the other by a computer-controlled linear positioning stage. The pump pulses are linearly polarised. When we control their mutual polarisation, a quarter-wave plate is inserted in one arm of the interferometer, and after passing through the plate twice (back and forth) the polarisation direction of one pulse is rotated by a chosen angle with respect to the other. When Fourier-transformed pulses are used, the pump field is often strong enough to induce multiphoton or tunnelling ionisation. The ionisation is unwanted because it competes with the NAREX process, even though it is useful to monitor the overlap between the pump and the molecular beams. Thus, the pump pulses are usually chirped to stretch the duration to >100 fs, by changing the position of the compressor grating in the fs laser system.

State-selective probes have been carried out by using ns dye laser systems as a frequency-tunable pulse source. The molecules examined so far have been nitric oxide (NO) [51,52,55,56] and benzene [53–55,57]. They have been probed by (1 + 1) REMPI *via* the $A^2\Sigma^+ \leftarrow X^2\Pi_{1/2}$ (0,0) band (at ~226 nm) and the $S_1 \leftarrow S_0 6_0^1$ band (at ~258 nm), respectively. In experiments on NO, the rotational lines were almost fully resolved with the grating scan providing a bandwidth of ~0.4 cm^{-1}. The pulse bandwidth was reduced to 0.05 cm^{-1} by inserting an etalon in the dye laser for resolving the much congested rotational structure of C_6H_6. The time delay between the pump and the probe pulses was fixed to 100 ns. Collisional rotational relaxation was negligible on this time scale. The polarisation direction of the probe pulses was set along with the ion extraction field for TOF-MS. Another issue for attention is the spatial overlap between the pump and probe pulses. It certainly matters for all of the pump–probe experiments, but it is very crucial in studies on NAREX, since the degree of excitation depends significantly on the pump field strength. Thus, we made the pump pulses loosely focused by a plano-convex lens with $f = 300$ mm, and its focal position was slightly shifted from the probe region.

On the other hand, the probe pulse was reduced down to 10 μJ/pulse, and tightly focused with a plano-convex lens with $f = 170$ mm. The spatial profile of the pump beam has been monitored at the probe position by a CCD camera; it has an oval shape with 80 μm × 100 μm (FWHM). The probe-beam spot size has been measured by the knife-edge method to have an FWHM of 26 μm × 29 μm. These results verify that a molecular ensemble exposed by a relatively uniform pump field has been probed. To optimise the spatial overlap between the pump and the probe beams, we first monitored the enhancement of ionisation by the pump pulse, by temporally overlapping the two pulses. Then, after setting back the appropriate delay, the beam position was slightly adjusted by maximising the rotational excitation.

5. Studies on nonadiabatic rotational excitation by state-resolved probe

5.1. *Nitric oxide*

The first state-resolved measurement on NAREX was reported on NO [51]. The molecule has been selected as a prototypical diatomic with suitable access *via* REMPI. Figure 5 shows an example of the $A^2\Sigma^+ \leftarrow X^2\Pi_{1/2}$ (0, 0) band of NO recorded at various pump pulse energies. Because of an efficient adiabatic cooling ($T_{rot} < 2$ K), almost the whole of the population has been concentrated to the lowest state, $J = 0.5$ in the $|\Omega| = 1/2$ manifold (the lower spin-orbit F_1 sublevel). This is evidenced by the spectrum measured without the pump [panel (a)], which exhibits only three lines sharing the common lower state, i.e. $J = 0.5$. The upper spin–orbit F_2 manifold with $|\Omega| = 3/2$ locates at ~120 cm^{-1} higher than F_1, and no transition from F_2 has been observed. Panels (b)–(d) correspond to the spectra measured with pump energies of 0.17, 0.35 and 0.62 mJ, respectively. The new spectral lines appeared when a pump field was applied. Transitions from states with the maximum

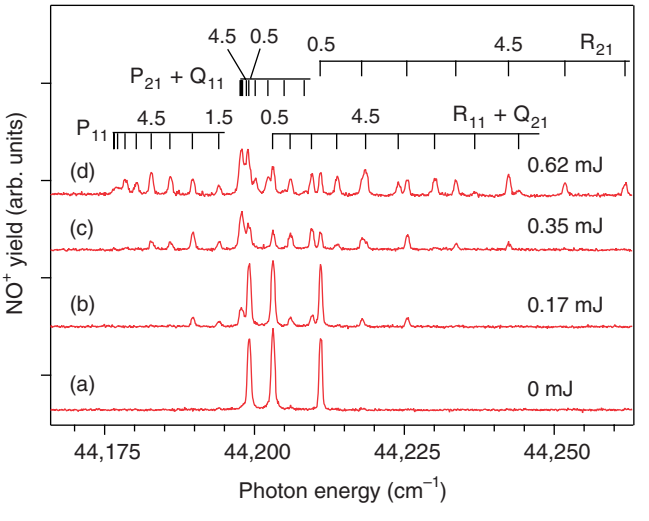

Figure 5. [Colour online] (1 + 1) REMPI excitation spectrum of the $A^2\Sigma^+ \leftarrow X^2\Pi_{1/2}$ (0, 0) band of NO after the irradiation of a nonresonant ultrafast laser pulse with various energies. The pulse duration was 150 fs. From Ref. [51].

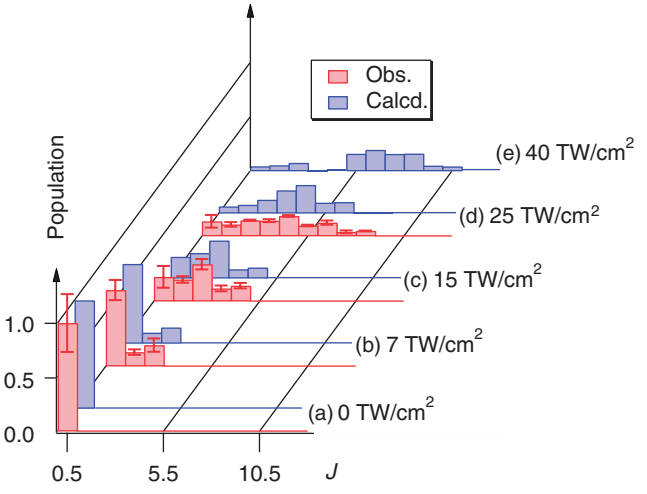

Figure 6. [Colour online] Rotational-state distributions of NO ($X^2\Pi_{1/2}$) after the irradiation of a nonresonant ultrafast laser pulse. Distributions for 0, 7, 15 and 25 TW/cm^2 correspond to panels (a)–(d) of Figure 5, respectively. From Ref. [51].

J up to 2.5, 4.5 and 8.5 were observed for the applied pump energies. From the observed spectra, the rotational-state distribution in $X^2\Pi_{1/2}$ has been derived, as shown in Figure 6. It is evident in this figure that the state distribution was spread among a wider range of J from the initial distribution confined to the single $J=0.5$ state, and its peak shifted to higher J values as the pump laser intensity was increased. More remarkably, the state distribution observed in NO ($X^2\Pi_{1/2}$) does not vary smoothly against J. For instance, states with $J=2.5$, 4.5 and 6.5 have a larger population than the adjacent $J=1.5$, 3.5 and 5.5 states.

In order to investigate the NAREX process of NO ($X^2\Pi_{1/2}$), a numerical simulation based on TDSE has been performed, as outlined in Section 3. The time-dependent wave function is expanded as Equation (28), with parity-adopted Hund's case (a) basis set, $\left|X^2\Pi_{1/2}; J, |\Omega|, M, \pm\right\rangle$, which is represented as

$$|J, |\Omega|, M, \pm\rangle = \frac{1}{\sqrt{2}}\left[|J, |\Omega|, M\rangle \pm (-1)^{J-1/2}|J, -|\Omega|, M\rangle\right]. \tag{45}$$

The eigen energy of a molecule is represented as

$$E_r = E_J = B(J-1/2)(J+3/2) \pm \sqrt{4B^2(J-1/2)^2 + A(A-4)} \mp (A-2B), \tag{46}$$

with A and B being the spin–orbit coupling and rotational constants, respectively, and the + sign corresponds to levels in F_2, while − to F_1. Here, Λ-doubling and centrifugal-distortion terms are not included, since their contribution is negligible. Thus, each J state is doubly degenerate with different parities. Because A ($=123.13\,\mathrm{cm}^{-1}$) $\gg B$ ($=1.696\,\mathrm{cm}^{-1}$) for NO ($X^2\Pi$) $v=0$ [172], Equation (46) can be approximated with sufficient accuracy for low-J states in the F_1 manifold,

$$E_J = B(J+1/2)^2, \tag{47}$$

after omitting the terms independent of J. Because the total Hamiltonian is invariant to inversion in space, $|\Psi_{r_i}(t)\rangle$ in Equation (28) has definite parity, and is composed of bases with the same parity. In addition, when the linearly polarised laser field (along the space-fixed Z-axis) is adopted, M is also preserved. The matrix elements for the laser–field interaction are nonvanishing only for $\Delta J = 0$, ± 1 and ± 2. The $\Delta J = \pm 1$ coupling is only allowed for linear molecules in a degenerate electronic or vibrational state, like NO ($X^2\Pi$), where each rotational state with a certain J is composed of a degenerate Λ (or l)-doubling pair. The matrix elements for $\pm$ parities are the same. In addition, changing the sign of M produces no effects on the matrix elements (aside from the phase). Thus, the time-dependent wave functions with different parities are identical to each other, and those with $M = +0.5$ and -0.5 are also. The coupled differential Equations (32) were numerically solved starting from, e.g. $|r_i\rangle = |J = 0.5, |\Omega| = 0.5, M = 0.5, +\rangle$. The results are also shown in Figure 6. The observed rotational-state distributions at 0.17, 0.35 and 0.62 mJ agree well with the calculated ones having laser intensities of 7, 15 and 25 TW/cm^2.

The time evolution of the probability densities, $|C_{r_i,r}(t)|^2 = [A_{r_i,r}(t)]^2$, of NO irradiated by a fs laser pulse with various laser intensities is shown in Figure 7. The figure shows a stepwise evolution from the initial state to higher-J states, which is induced by a Raman-type excitation process governed by the interaction with the laser field. Even though each excitation only involves changes in J by 1 or 2, such excitations can proceed successively to transfer the population from low-J to higher-J states until the laser field diminishes. As the laser intensity is increased, the build-up (and the subsequent fall-off) of rotational populations for each states becomes faster and, as a consequence, excitation to higher-J states is achieved.

A detailed examination of Figure 7 reveals a characteristic phenomenon in the rotational-state evolution in NO ($X^2\Pi_{1/2}$): pairs of adjacent states, $\{1.5, 2.5\}$, $\{3.5, 4.5\}$, $\{5.5, 6.5\}$ and so on, show an almost identical time dependence, and the population of 1.5 (3.5, 5.5, ...) is smaller than that of 2.5 (4.5, 6.5, ...). This fact is explained as follows: because $\Delta J = 1$ and 2 couplings are allowed, the initial population of $J = 0.5$ is transferred to states with $J = 1.5$ and 2.5 almost simultaneously in the first excitation step. Subsequent excitations with $\Delta J = 1$ and 2 further transfer the population to higher-J states in a stepwise manner. However, the coupling strengths become dominant for $\Delta J = 2$ over those for $\Delta J = 1$ as J increases, as shown in Figure 8. Therefore, most of the population from $J = 1.5$ is transferred to $J = 3.5$, while $J = 2.5$ to $J = 4.5$. As a result, the state population is nonadiabatically transferred *via* two separate excitation pathways, starting from the common initial state, $J = 0.5 \rightarrow 1.5 \rightarrow 3.5 \rightarrow 5.5 \rightarrow \cdots$ and $J = 0.5 \rightarrow 2.5 \rightarrow 4.5 \rightarrow 6.5 \rightarrow \cdots$ Because the population transferred in the first step is smaller in the former pathway, the subsequent states also have a smaller population than those in the latter pathway. The existence of the two distinct excitation pathways directly cause the previously mentioned dominating population for 2.5, 4.5, ... in the observed state distribution of NO ($X^2\Pi_{1/2}$).

Experiments utilising the double-pulse excitation by Meijer *et al.* [52] have provided a clear verification of the bifurcated excitation pathways in the NAREX of NO ($X^2\Pi_{1/2}$). We have also performed quite similar experiments [55,56,173]. The delay-time dependence of the rotational-state distribution was examined as the REMPI signals for each transition with different J values, as shown in Figure 9. Characteristic modulations in population are observed against the delay, and the modulation patterns differ from one another for different J. The delay-time dependence of the rotational-state distribution was calculated

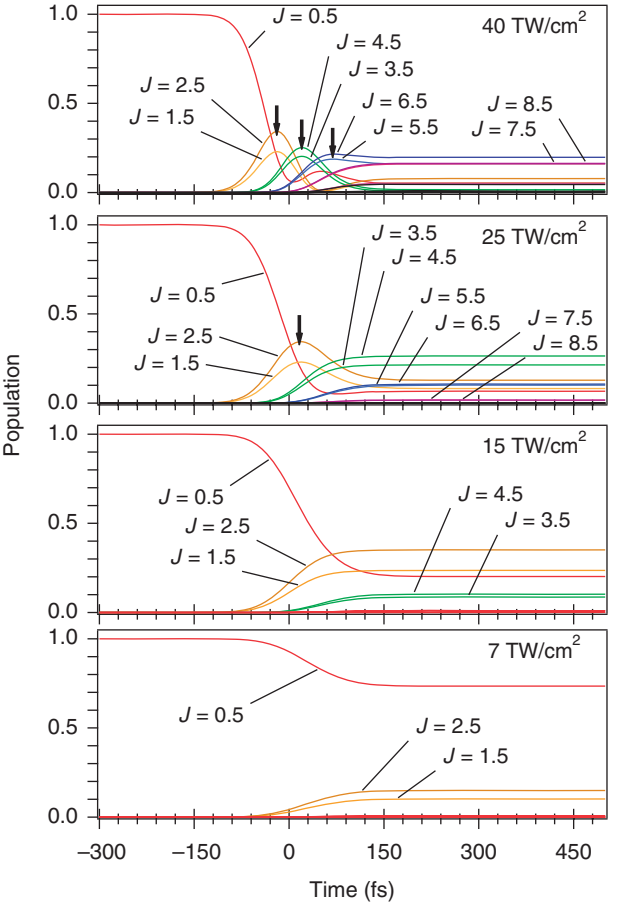

Figure 7. [Colour online] Time evolution of the probability densities of NO irradiated by a nonresonant fs laser pulse with various energies. From Ref. [51].

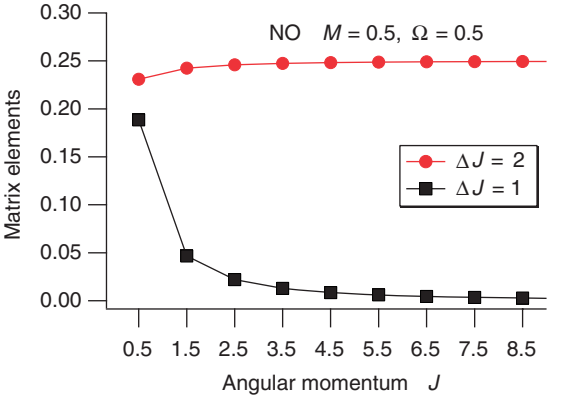

Figure 8. [Colour online] Coupling matrix elements for nonadiabatic rotational excitation in NO ($X^2\Pi_{1/2}$). From Ref. [53].

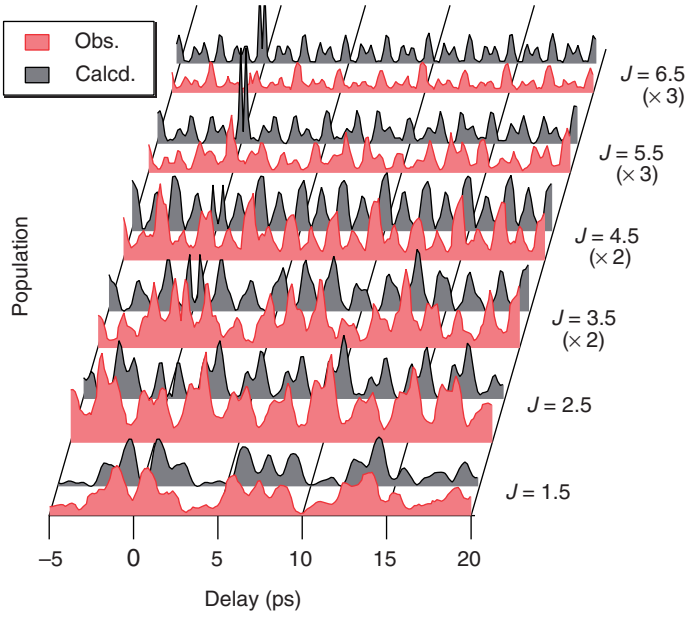

Figure 9. [Colour online] Population of each rotational level of NO ($X^2\Pi_{1/2}$) irradiated by a nonresonant intense fs double-pulse pair, plotted against the delay between the two pulses. From Ref. [55].

by applying Equation (40), with the amplitudes and phases numerically evaluated by solving the coupled differential equations presented in Equation (5). The results are also represented in Figure 9. The agreement between the experiment and the calculation is remarkably good.

Figure 10(a) displays the Fourier-transformed signals of the observed beat signals for $J = 1.5$–6.5. As expected, the peaks appear at the positions corresponding to the rotational energy differences, as shown in panel (b). The peak assignments are also shown at the top of panel (a). It is noted that the rotational wave packet created *via* NAREX from the initial $|J = 0.5, |\Omega| = 0.5, M = \pm 0.5, \pm\rangle$ state is a coherent superposition of eigenstates with J ranging from 0.5 to 6.5, having the same parity and M value. These states are grouped into two according to the excitation pathways, as mentioned before. The existence of two different groups of states is clearly seen in Figure 10(a). One of them, here referred to as group I ($J = 2.5$, 4.5 and 6.5), has common peaks, such as $8B$, $16B$, $24B$ and $40B$, while the other group II ($J = 1.5$, 3.5 and 5.5) exhibits peaks at different positions, such as $3B$, $12B$, $15B$, $20B$ and $32B$. This exclusive nature among the two groups is a direct consequence given in Equation (40), which shows that the beat amplitude appearing at $\Delta\omega_{r',r''}$ is proportional to $A_{r_i,r'}A_{r',r}A_{r_i,r''}A_{r'',r}$ when probing the population of $|r\rangle$ with the initial state $|r_i\rangle$. When all of the three states $|r\rangle$, $|r'\rangle$, $|r''\rangle$ belong to the same group, all of the transition amplitudes have appreciable values, but if one of the three, say, $|r'\rangle$, belongs to a different group, $A_{r',r}$ is almost negligible. These situations, as illustrated in Figure 11, are another quantal correspondence to the well-known Young's double-slit experiment, in which interference appears when the initial and final points are connected *via* two independent paths, but it vanishes if one of them is blocked.

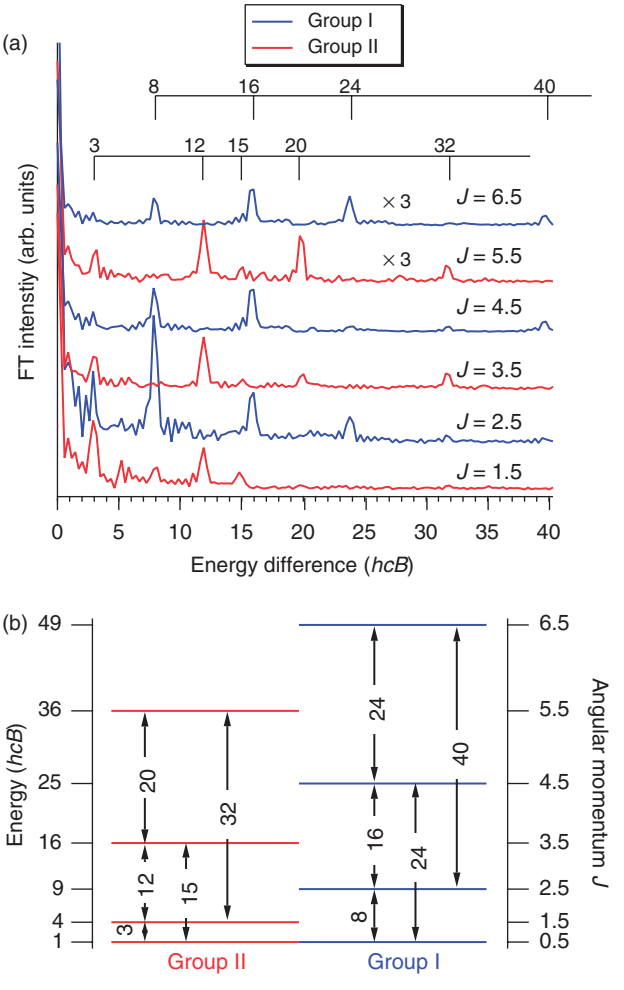

Figure 10. [Colour online] (a) Power spectra of the delay-dependent populations of each rotational level, and (b) energy-level diagram of NO ($X^2\Pi_{1/2}$) and the excitation pathways in the nonadiabatic rotational excitation from the $J=0.5$ initial state. From Ref. [55].

The delay-time dependence of the rotational-state distribution exhibits a noteworthy feature. The state distribution changes periodically with the interval of ≈20 ps. This revival time is twice larger than the well-known value, $T_{\rm rev}=1/(2Bc)$ [14–21]. This difference originates from the energy level structure of NO. For a linear molecule in nondegenerate electronic states, such as N_2, O_2 and CO_2, the angular momentum J is an integer. Thus, the rotational energy, $E_J/hc=0, 2B, 6B, 12B, \ldots, BJ(J+1)$, has the greatest common measure (GCM) of $2B$. The rotational wave packet represented in Equation (28) is invariant under the time evolution from t to $t+T_{\rm rev}$ because $\exp(-i\omega_r T_{\rm rev})=1$. On the other hand, molecules in degenerate electronic states, such as NO and OH, have a half-integer angular momentum, J. The rotational energy is approximately given in Equation (47), with the GCM of B. The rotational wave packet of those molecules returns to the initial value by time evolution from t to $t+1/(Bc)$.

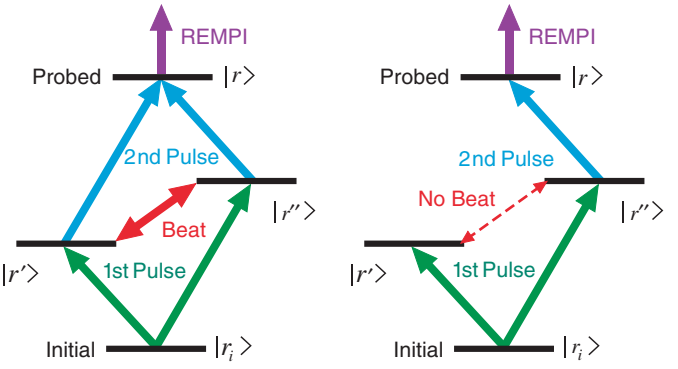

Figure 11. [Colour online] Schematic diagram explaining the appearance and the absence of a certain beat component in the delay-dependent rotational-state populations of NO ($X^2\Pi_{1/2}$) irradiated by a nonresonant intense fs double-pulse pair.

Another important upshot from the double-pulse excitation studies is control of the rotational-state distribution. Meijer *et al.* [52] have shown numerically that each of the two excitation pathways can be selected by choosing a delay time τ between the two excitation pulses. This selectivity can be explained in a simplified manner, as follows. We first consider the two-level system with eigenstates, $|r_i\rangle$ and $|r\rangle$. Then, the population for the latter state is expressed as

$$\left|B_{r_i,r}(\tau)\right|^2 = \left(A_{r_i,r}\right)^2\left[\left(A_{r_i,r_i}\right)^2+\left(A_{r,r}\right)^2+2A_{r_i,r_i}A_{r,r}\cos\left(\Delta\omega_{r,r_i}\tau+\delta_{r_i,r_i}-\delta_{r,r}\right)\right]. \qquad (48)$$

If the two-phase factors are assumed to be not very different, the state population is completely depleted at $\tau = 2\pi(n+1/2)/\Delta\omega_{r,r_i}$ ($n=0,1,2,\ldots$). For the first excitation steps from $J=0.5$ to $J=1.5$ or 2.5, $2\pi/\Delta\omega_{r,r_i} = 1/(3Bc)$ or $1/(8Bc)$, respectively. Then, when τ is set to, for instance, $1/(2Bc)$, the population of $J=1.5$ is minimised while that of $J=2.5$ is maximised. This difference in the initial steps leads to an enhancement or depletion in each of the two excitation pathways. Of course, in reality, more than two eigenstates are involved in the wave-packet creation and the two-level treatment is less adequate. Then, a complete selection can be rarely accomplished, except for ideal two-level systems. Still, in some cases, a high degree of selectivity will be realised by properly choosing the delay and the intensity of the excitation pulses. Typical numerical results are shown in Figure 12. At $\tau = 10.4\,\text{ps} \approx 1/(2Bc)$, more than 70% of the population is concentrated to a single state, $J=2.5$. Interestingly, the population can also be concentrated to the initial state, $J=0.5$, for $\tau = 4.2\,\text{ps}$. The delay time is roughly close to 1/2 of $1/(3Bc)$ and 3/2 of $1/(8Bc)$, which fulfil the depletion condition for $J=1.5$ and 2.5, respectively. When a quantum state after the sequential interactions with two identical pulses goes back to the initial state, the two pulses are called a 'zero effect pulse pair (ZEPP)' [36]. ZEPPs are regarded as being highly important in information processing based on molecular quantum states.

5.2. *Benzene*

Benzene (C_6H_6) has been selected as the second molecule for the state-resolved measurement on NAREX [53]. The molecule is a prototypical symmetric top, possessing

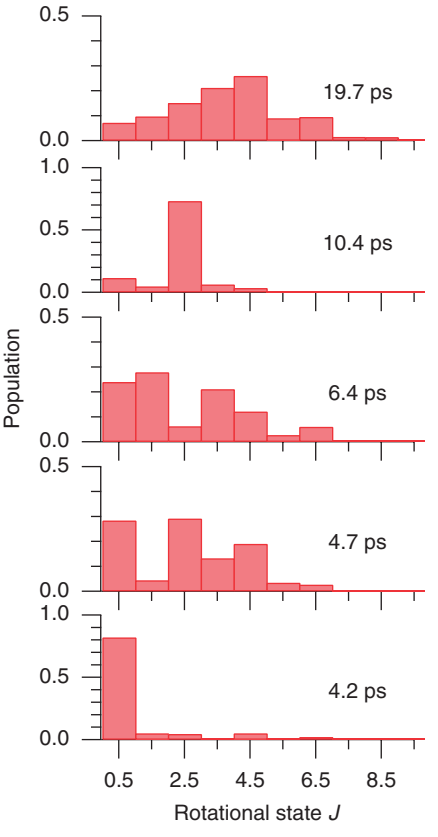

Figure 12. [Colour online] Rotational-state distributions of NO ($X^2\Pi_{1/2}$) after the irradiation of a fs double-pulse pair, calculated for various delay times. Field strength is 34 TW/cm^2 for each pulse and the pulse duration is 150 fs.

the other rotational degree of freedom than linear or diatomic molecule. As mentioned in Section 3, the selection rules for level coupling in NAREX are rather strict for symmetric tops, and make it greatly simple to track the excitation pathways. Still, a rich variety in the excitation processes has been expected. Figure 13 shows the $(1+1)$ REMPI excitation spectra of the $S_1 \leftarrow S_0$ 6_0^1 band measured with and without pump pulses. As mentioned in Section 4, the spectrum without a pump is predominated by transitions only from the lower rotational states of $(J,K)=(0,0)$, $(1,0)$, $(1,1)$, $(2,2)$ and $(3,3)$, because of the efficient rotational cooling to 0.5 K. Due to the D_{6h} symmetry of the molecule, rotational levels with $K=6n$, $6n\pm1$, $6n\pm2$ and $6n\pm3$ (n being an integer) are associated with nuclear spin wave functions with B_1+B_2, E_2, E_1 and A_1+A_2, symmetries, respectively. For $K=0$, even and odd J levels are assigned to B_1 and B_2 [168]. Nuclear spin conversion during collisions is inefficient, so that molecules with different nuclear spin symmetries can be regarded as different molecular species, i.e. 'nuclear spin isomers' [38,131]. The observed five states are the lowest rotational states for the corresponding nuclear spin isomers.

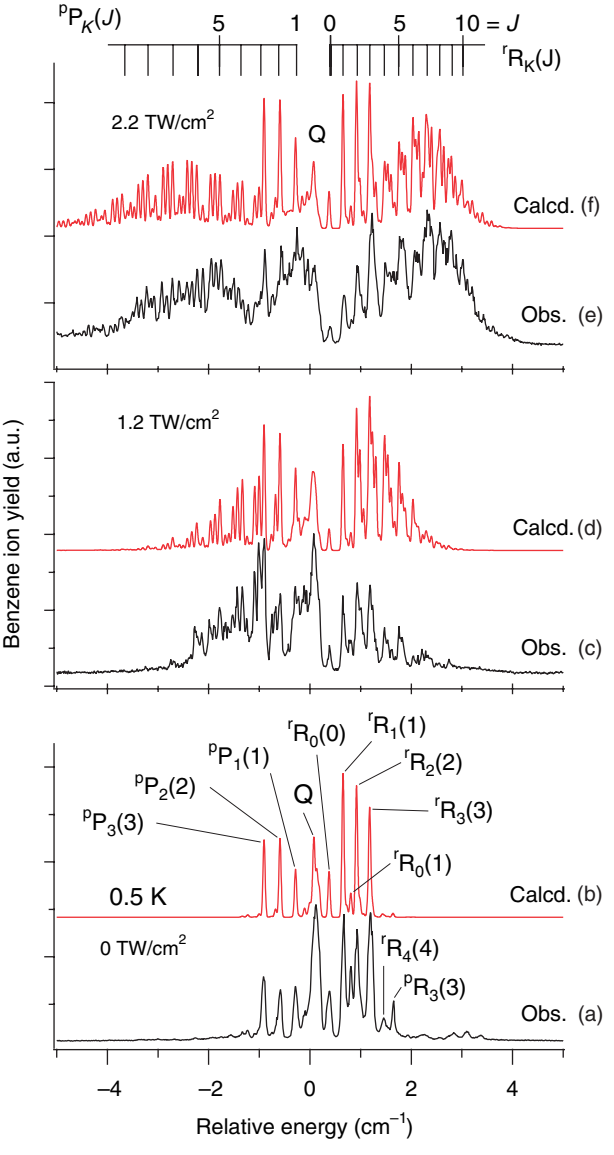

Figure 13. [Colour online] (1 + 1) REMPI excitation spectrum of the $S_1 \leftarrow S_0$ 6_0^1 band of benzene after the irradiation of a nonresonant ultrafast laser pulse with various energies. The pulse duration was 700 fs. From Ref. [53].

The excitation spectra changed drastically when the pump pulses of 1.25 and 2.4 mJ were applied, as shown in Figure 13. Transitions from states with the maximum J up to 6 and 10 appeared for 1.25 and 2.4 mJ, respectively. In the figure, a series of triplet lines are recognised, particularly in the ^{p}P-branch. These characteristic triplet lines are assigned to transitions from states with $K = 1$, 2 and 3. This is the consequence of the initial distribution restricted to $K = 0$–3, with small contributions from $K \geq 4$ (1%), and the

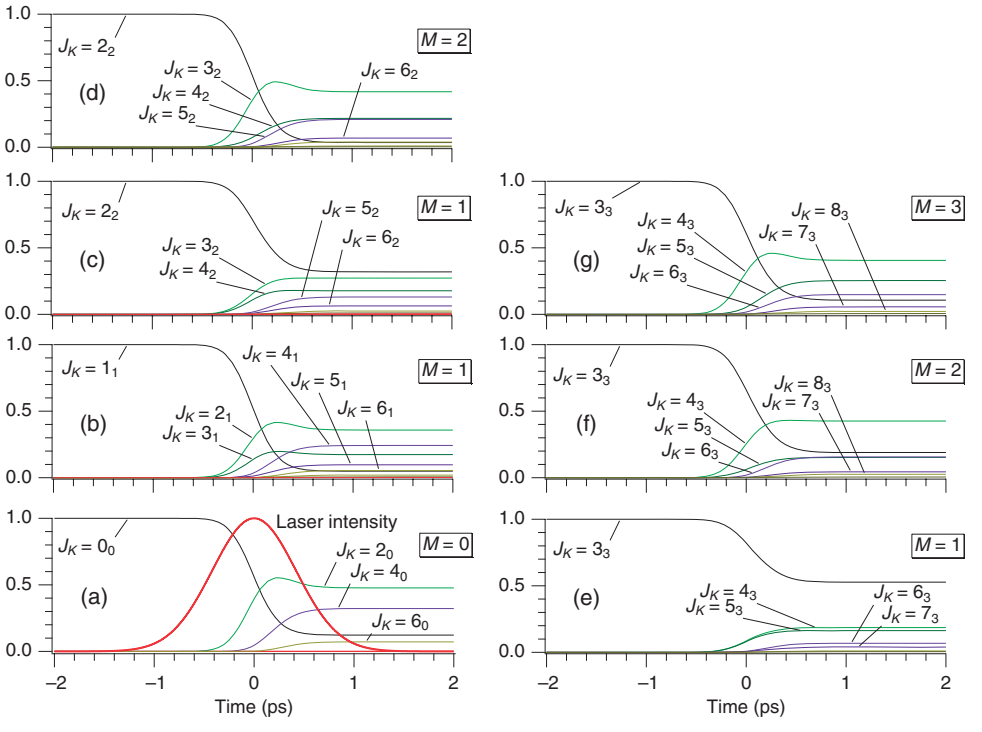

Figure 14. [Colour online] Time evolution of the probability densities starting from various initial states, calculated for benzene. The pump intensity is 1.2 TW/cm^2 and the pulse width is 700 fs.

conservation of K in the NAREX process, as mentioned before. A quantum dynamical calculation outlined in Section 3 has been performed to compare the observed spectra with calculated ones on the basis of the population determined by solving TDSE. Figure 13 shows the calculated spectra, for which the pump intensities of 1.2 and 2.2 TW/cm^2 are used with the 700 fs pulse duration. The match-up to the observed spectra is satisfactory.

The dynamical calculation has provided the time evolution of the probability densities from several initial states of C_6H_6, as shown in Figure 14. The figure demonstrates the systematic changes in the excitation pathways, depending on the quantum numbers. When the initial states are those with $K=0$ and/or $M=0$, excitation proceeds in a stepwise manner with $\Delta J=2$ to higher-J levels. These NAREX dynamics are identical to those in linear molecules. In the case of $KM\neq 0$, the excitation processes become more involved, due to the additional $\Delta J=1$ transitions. For $M=1$, pairs of adjacent states show almost the same time evolution, which looks quite similar to the bifurcated excitation pathways in NO ($X^2\Pi_{1/2}$), as mentioned before. The only difference is the predominance of $\Delta J=1$ over $\Delta J=2$ in the first steps for C_6H_6, while the major pathway starts with $\Delta J=2$ for NO. On the contrary to the states with $M=1$, higher-M states exhibit sequential build-up of populations with $\Delta J=1$. These excitation processes are governed by the relative sizes of the coupling matrix elements. As a result, the population transfer in the $K=1$ stack proceeds in two different pathways, while all the subsequent J levels are connected to each

other in the $K=2$ and 3 stacks. Such details in the NARAX process of C_6H_6 have recently been explored in double-pulse excitation experiments [174].

It is noted that NAREX from the $(J, K)=(0, 0)$ state results in the populations of states with $K=0$ and even J concentrated into the single $M=0$ sublevel. Similarly, since the excitations from $(J, K)=(1, 1)$ with $M=0$ into even J states are forbidden, populations for $K=1$ with even J come solely from the initial state with $M=\pm 1$. Such highly polarised rotational states will be utilised for various studies on reaction dynamics; for instance, rotational state-selective measurements of the alignment dependence on photoionisation or photodissociation.

5.3. *Rotational wave-packet reconstruction*

If we probe the population of the initial state after the double-pulse excitation, Equation (40) reduces into

$$\left|B_{r_i,r_i}(\tau)\right|^2=\sum_r \left(A_{r_i,r}\right)^4+2\sum_{r>r'}\left(A_{r_i,r}\right)^2\left(A_{r_i,r'}\right)^2\cos\left[\Delta\omega_{r,r'}\tau+2\left(\delta_{r_i,r}-\delta_{r_i,r'}\right)\right]. \qquad (49)$$

Thus, a series of measurements on the population by varying τ allows us to determine the set of amplitudes, $A_{r_i,r}$, and phases, $\delta_{r_i,r}$, for the constituent eigenstates. It is nothing but an experimental reconstruction of the rotational wave packet created *via* NAREX by a nonresonant ultrafast laser pulse. Quantum-state reconstruction of a wave function has been a key issue in contemporary physics for over more than a decade [175–177]. Several studies have reported its experimental realisation for atomic/molecular systems [178–182]. In these studies, the field–matter interaction is well within the perturbative regime. There was only a single proposal concerning a tomographic reconstruction for a time-dependent quantum state, generated nonadiabatically by an intense ultrafast laser pulse [183]. The proposed reconstructing procedure is based on observations of the polar angular distribution, which is totally different from that by the measurements of $\left|B_{r_i,r_i}(\tau)\right|^2$.

To demonstrate quantum-state reconstruction by time-dependent population measurements, benzene molecules have been selected as a sample to be examined [54]. Here, the A_1 nuclear-spin species has been focused. The initial-state distribution in the A_1 manifold is concentrated mostly to the $(J, K)=(0,0)$ state (>96% in the condition of $T_{\mathrm{rot}}\sim 0.5\,\mathrm{K}$), and this state contains only a single M (=0) sublevel. Thus, we regard it as being a good approximation that the initial molecular ensemble in this nuclear-spin manifold is in a pure state, $|r_i\rangle=|J_i, K_i, M_i\rangle=|0, 0, 0\rangle$. To measure the population denoted in Equation (49), REMPI signals have been recorded by fixing the probe pulse on the ${}^rR_0(0)$ transition, while scanning the delay, τ. A typical example of the observed signal is shown in Figure 15. This trace was least-squares fitted to Equation (49) to determine the amplitudes and phases, with the beat frequencies, $\Delta\omega_{r,r'}$, fixed to those obtained from the precisely known rotational constants. Excitation to states with $J>8$ are negligibly small, so five eigenstates ($J=0$, 2, 4, 6 and 8 with $K=0$) were included in the analysis. Because of the normalisation condition on the population, the sum of the squares of the amplitudes should be unity. This constraint was taken into account in the fit. Since $\left|B_{r_i,r_i}(\tau)\right|^2$ depends on not the values of each phase, but the phase differences, $2\left(\delta_{r_i,r}-\delta_{r_i,r'}\right)$, the choice of $\delta_{r_i,r_i}=0$ was adopted. Figure 16 shows the determined phase and population for each J state. It is noted that the determined phase has an uncertainty of π because the addition of

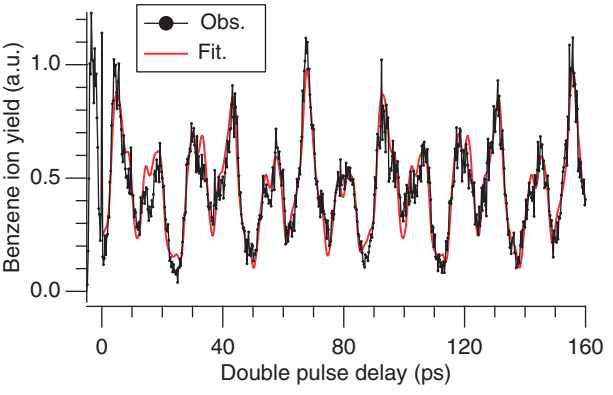

Figure 15. [Colour online] Population of the $(J, K) = (0, 0)$ state of benzene irradiated by a nonresonant intense fs double-pulse pair, plotted against the delay between the two pulses. From Ref. [54].

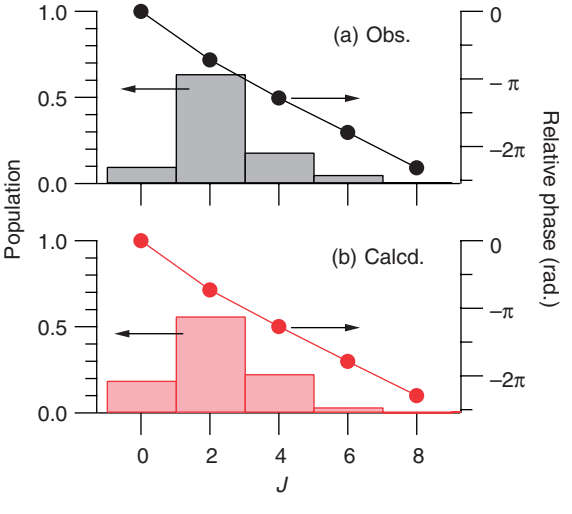

Figure 16. [Colour online] Population and phase for each eigenstate, constituting the wave packet created by the nonadiabatic rotational excitation from the $(J, K) = (0, 0)$ state of benzene Panel (a) is the results from least-squares fitting of the experimental trace shown in Figure 15. Panel (b) is those derived from the TDSE calculation. From Ref. [54].

π gives the same value for $\left|B_{r_i,r_i}(\tau)\right|^2$. Hence, an appropriate choice can be made by a comparison with the calculation mentioned below.

As can be seen in Figure 15, $\left|B_{r_i,r_i}(\tau)\right|^2$ almost (but not perfectly) revives (i.e. reaches to unity) at certain delay times, i.e. $68\,\text{ps} + nT_{\text{rev}}$ where $T_{\text{rev}} = 88\,\text{ps}$ for benzene. When the probe laser sampled a wider region with a nonuniform pump field, the extent of the revivals was greatly reduced because of the inhomogeneous dephasing inherent in a mixed state, created by the varying field, even though the initial state was a pure state. In this case, the sum of the determined $|A_J|^2$ without any constraint for the normalisation in

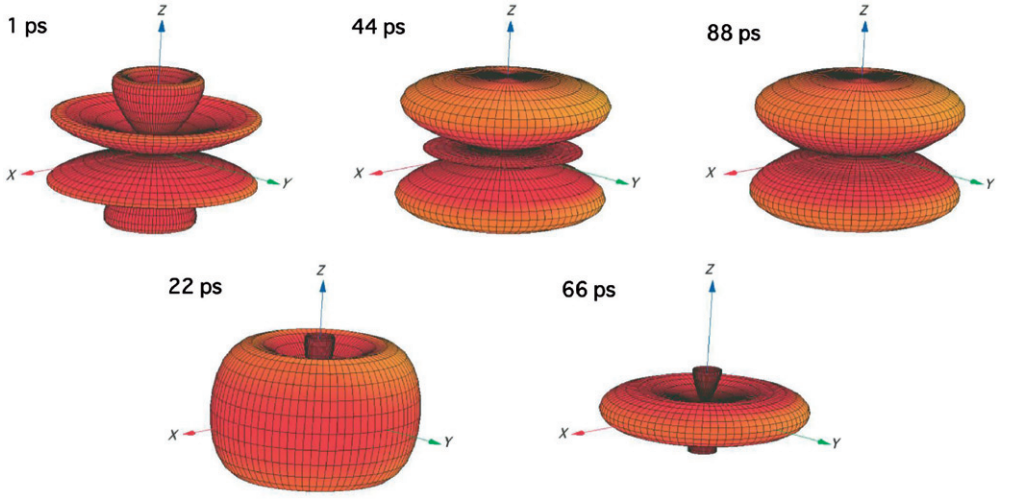

Figure 17. [Colour online] Reconstructed rotational wave packet of benzene, created from the $(J, K) = (0, 0)$ initial state by the excitation of the nonresonant fs laser pulse. The laboratory-frame probability distribution for the molecular symmetry axis is indicated for several delay times. From Ref. [55].

population became much less than unity. For the trace shown in Figure 15, the sum of the population reached to 0.97, validating the creation of a wave packet by an intense laser field with acceptable uniformity.

The phases and population calculated by solving the TDSE are also displayed in Figure 16. Here, the pump laser intensity was adjusted so as to best reproduce the observed phase and amplitude. The thus-obtained value ($10\,\mathrm{TW/cm^2}$) reasonably agrees with that ($8.4\,\mathrm{TW/cm^2}$) evaluated from the experimental parameters (pulse energy, duration and spot size). As shown in Figure 16, the calculation satisfactorily reproduced the experimental results. The phase determined in the rotational wave packet retrieval decreases monotonically as J becomes larger. This is a clear experimental signature for the stepwise excitation pathway during the interaction with the laser field, $J = 0 \rightarrow 2 \rightarrow 4 \rightarrow \cdots$ in the $K = 0$ stack, obeying the rotational Raman selection rule of $\Delta J = \pm 2$. In the case of the weak-field limit, the phase difference between two states coupled with the lowest-order Raman process (proportional to the square of the field) is $-\pi/2$ (or $\pi/2$) for negative (or positive) $\Delta\alpha$. However, when the field is large enough to go beyond the perturbative regime, the phase shift substantially deviates from the limiting value.

Once all of the phase and the amplitude for each constituent eigenstate is experimentally retrieved, the spatial distribution for the rotational wave packet can be evaluated at an arbitrary delay time. As representatives, the angular probability distribution is indicated for some delay times in Figure 17. The phase, as well as the amplitude, certainly controls the wave-packet dynamics. For instance, if $\delta_{0,J+2} - \delta_{0,J} = -\pi/2$, as in the limiting case mentioned above, $\left|B_{r_i,r_i}(\tau)\right|^2$ becomes unity when $\tau = (n + 1/2)T_{\mathrm{rev}}$; so the two pulses are a ZEPP. In an actual situation, $\left|B_{r_i,r_i}(\tau)\right|^2$ at $(n + 1/2)T_{\mathrm{rev}}$ reaches only to 0.86, while the maximum (0.98) appears at 68 ps ($+nT_{\mathrm{rev}}$).

The substantially different delays from $(n+1/2)T_{\mathrm{rev}}$ for the approximate ZEPPs are definitely due to the phase shifts in the nonperturbative regime.

The double-pulse excitation coupled with the state-specific probe on the initial state, described here, is the first experimental retrieval of a quantum state created by the matter–field interaction beyond the perturbative regime. In the previous proposal for quantum-state reconstruction [183], a polar angular distribution of the molecular ensemble is expected to be used. Such data can be obtained *via*, for instance, photofragment ion imaging. In cases of polyatomic molecules, however, care must be paid for effects of any dissociation dynamics, i.e. the fragment velocity distribution in the molecular frame. In addition, an initial ensemble in a single quantum state must be prepared, since all the molecules are subjected by photodissociation. On the other hand, the present reconstruction relies on a modification of the initial wave packet by the second laser pulse, free from possible dynamical effects in the probe process. It is not necessary to prepare a single-state initial ensemble, thanks to the quantum-state-resolved probe to select an appropriate state out from a mixed ensemble. This is a great advantage, particularly when we will apply it to asymmetric-top molecules, for which state selection *via*, e.g. hexapole filtering is practically very difficult.

5.4. *Ultrafast angular-momentum orientation*

Most of the studies so far reported on NAREX have been related to the alignment of the rotational angular momenta in a molecular ensemble, yet irrelevant to the angular-momentum orientation. There have been two reports on the orientation by irradiation of nonresonant short pulses [148,184], but the duration of the excitation pulses implemented therein were comparable to, or longer than, the rotational periods, so that these studies were performed rather within the adiabatic regime. On the other hand, stationary spectroscopic approaches implementing one- or two-photon resonant transitions have been extensively applied to the realisation of the angular-momentum orientation [13,77]. The significance of the orientation is evident when we consider a classical vector model; the signed value of M corresponds to the angular velocity around the Z-axis, so that the creation of an oriented ensemble is to make the molecules rotate in the clockwise or counter-clockwise direction, as shown in Figure 18.

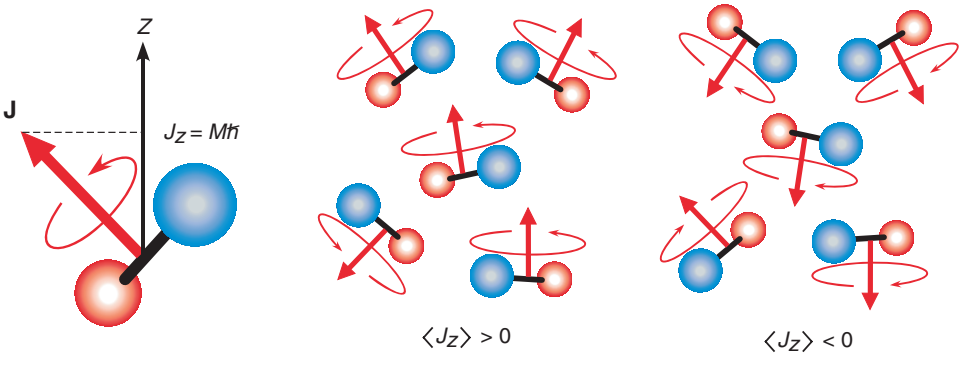

Figure 18. [Colour online] Classical vector model for angular momentum and the molecular ensembles exhibiting orientation.

In the previous studies of the orientation, circularly polarised radiations have been exclusively adopted to induce the required helical interaction that breaks the right/left-handed symmetry around the Z-axis. In the case of NAREX with nonresonant irradiation, however, a circularly polarised pulse cannot exert any torque around the Z-axis, as shown in Equations (23) and (24). Quite recently, it has been theoretically predicted [185] and experimentally verified [57] that NAREX with a pair of linearly polarised pulses can induce angular-momentum orientation when the mutual polarisation direction and the time delay between them are properly arranged. Here, we set the Z-axis along the laser propagation direction and the polarisation of the first pulse parallel to the X-axis. The second pulse is delayed by τ, and its polarisation is tilted against that of the first one by angle $\Delta\phi$, as shown in Figure 19. Here a symmetric-top molecule is taken as a sample. Then, the interaction with the first pulse is represented in Equation (19), and the expansion coefficient appearing in Equation (28) is calculated by the TDSE employing the interaction term. Of course, this single pulse excitation cannot bring any orientation, but the introduction of the second pulse breaks the right/left-handed symmetry. When the new axis system is defined so as the X' axis is set parallel to the polarisation of the second pulse, the new and old angular coordinates are related as: $\phi' = \phi - \Delta\phi$. Consequently, the symmetric-top wave function transforms as

$$|J, K, M\rangle \mapsto |J, K, M\rangle \exp(iM\Delta\phi) \tag{50}$$

By taking the transformation into account, the transition amplitude, $B_{r_i,r}$, in Equation (39) is rewritten, if the second pulse is a replica of the first one, as

$$B_{r_i,r}(\tau) = \sum_{r'} C_{r_i,r'} C_{r',r} \exp\left[-i\left(\Delta\omega_{r',r}\tau - M'\Delta\phi\right)\right], \tag{51}$$

where r' stands for the set of (J', K', M'). Because of the phase factor depending on the angle $\Delta\phi$ and M, the final populations for $+M$ and $-M$ may differ from each other. To clarify this, we here consider a simplified situation, where the laser field is weak enough

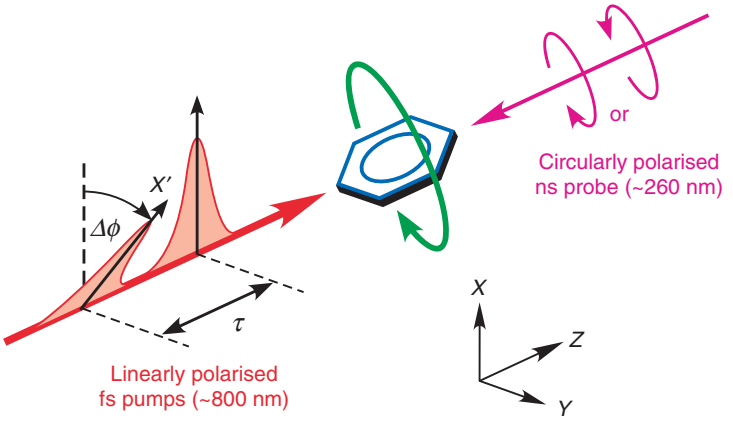

Figure 19. [Colour online] Experimental scheme for creating an oriented rotational wave packet by tilted double-pulse excitation. From Ref. [57].

to adopt a perturbative treatment. Then, the diagonal expansion coefficient is $C_{r,r} \approx 1$, while that for $r' \neq r$ is represented as

$$C_{r,r'}(t) = -i\hbar \int_{-\infty}^{t} \langle r|\hat{V}(t')|r'\rangle \exp\bigl(-i\Delta\omega_{r',r}t'\bigr)dt'. \tag{52}$$

The coefficient in Equation (52) is nonvanishing only when $M - M_i \equiv \Delta M = 0$ or ± 2 because of the selection rules for the interaction given in Equation (19). In the case of $\Delta M = \pm 2$, Equation (51) is approximated as

$$\begin{aligned} B_{r_i,r}(\tau) &= C_{r_i,r_i}C_{r_i,r}\exp\bigl[-i\bigl(\Delta\omega_{r_i,r}\tau - M_i\Delta\phi\bigr)\bigr] + C_{r_i,r}C_{r,r}\exp\bigl[-i\bigl(\Delta\omega_{r,r}\tau - M\Delta\phi\bigr)\bigr] \\ &\approx C_{r_i,r}\exp(iM\Delta\phi)\bigl\{\exp\bigl[i\bigl(\Delta\omega_{r,r_i}\tau \mp 2\Delta\phi\bigr)\bigr] + 1\bigr\}. \end{aligned} \tag{53}$$

This indicates that the populations for $M = M_i \pm 2$ may be different as a result of the interference between the different phase factors for the two pulses. It is noted that $\Delta\phi$ should neither be $\neq 0$ nor $\pi/2$, otherwise no orientation is created because of the mirror symmetry for the parallel or perpendicular polarisation arrangement. Equation (53) shows that complete constructive and destructive interferences are realised for $\Delta M = +2$ and -2, respectively, in the cases that $\Delta\phi = \pi/4$ and $\Delta\omega_{r,r_i}\tau = \pi/2 + 2\pi n$ or $\Delta\phi = -\pi/4$ and $\Delta\omega_{r,r_i}\tau = 3\pi/2 + 2\pi n$. For complete constructive and destructive interferences for $\Delta M = -2$ and $+2$, respectively, $\Delta\phi = \pi/4$ and $-\pi/4$ are interchanged under the conditions mentioned above, designating the exchange of the relative polarisations for the two pulses.

The aforementioned discussion based on the perturbative treatment has been validated by a numerical analysis with TDSE [57]. The molecular parameters for benzene [53] were adopted in the calculations. In Figure 20, final populations starting from $|0, 0, 0\rangle$ are plotted against the delay, τ, for $\Delta\phi = \pi/4$. When the laser-field intensity is relatively low ($0.1\,\mathrm{TW/cm^2}$), the populations for $|2, 0, \pm 2\rangle$ show completely anti-phase sinusoidal modulations to each other, exhibiting maximum or minimum (=0) at the expected delay times, $\tau = \pi/\bigl(2\Delta\omega_{J=2,J=0}\bigr) = 1/(24Bc) = 7.3\,\mathrm{ps}$ or $3\pi/\bigl(2\Delta\omega_{J=2,J=0}\bigr) = 1/(8Bc) = 21.9\,\mathrm{ps}$. For a much higher intensity ($1.6\,\mathrm{TW/cm^2}$), they come to show a substantial deviation from the dependence represented in Equation (53), because of coupling with other rotational states, which promotes population transfer to the higher levels *via* stepwise excitation. Still, large population differences between the $|2, 0, \pm 2\rangle$ states can be realised in the vicinity of the conditions mentioned above.

The feasibility of the double-pulse excitation with mutually tilted polarisations has been demonstrated with benzene as a sample molecule [57]. The experimental setup was quite similar to the double-pulse excitation experiments with a state-resolved probe adopted for NO, as mentioned in the previous section. One of the modifications was the insertion of a quarter-wave plate in one arm of the Michelson interferometer to control the polarisation of one of the excitation pulses. The other is the application of circularly polarised probe pulses to assess the degree of orientation for each rotational level after the double-pulse excitation. Figure 21 shows a typical example of the REMPI excitation spectra, recorded after excitation by the fs pulse pair, of which the mutual polarisation angle was set as $\pi/4$ or $-\pi/4$. The delay time (7.3 ps) is optimum in the low-field limit to achieve the largest orientation in the $(J, K) = (2, 0)$ and $(3, 2)$ states, i.e. $\tau = \pi/\bigl(2\Delta\omega_{J=2,J=0}\bigr) = \pi/\bigl(2\Delta\omega_{J=3,J=2}\bigr)$, as discussed before. Since the delay time also provided substantial population differences between the $\pm M$ sublevels in many other rotational states, e.g. $(2, 1)$, $(2, 2)$, $(3, 1)$ and $(4, 3)$, P-branch transitions from these states

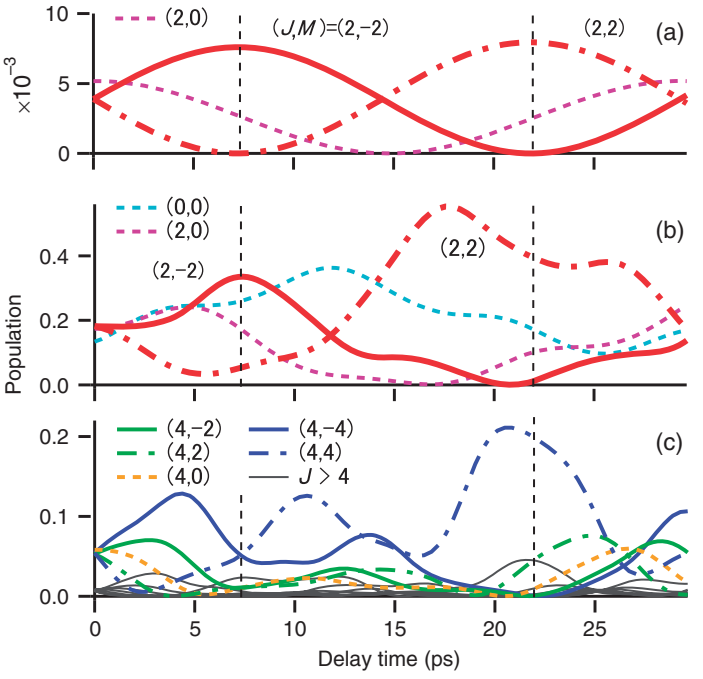

Figure 20. [Colour online] Populations from the $(J, K, M) = (0, 0, 0)$ initial state after the tilted double-pulse excitation. Field intensities are: 0.1 TW/cm^2 for (a) and 1.6 TW/cm^2 for (b) and (c). In panel (a), the population of $(J, M) = (0, 0)$ is out of the vertical scale. From Ref. [57].

showed pronounced intensity changes against the circularity of the probe pulse. This experimental finding verified the successful realisation of the angular-momentum orientation in the vibronic ground state of benzene. The relative intensities for the right- and left-handed probe conditions were entirely reversed when the polarisation angle was changed form $\pi/4$ or $-\pi/4$. This is a natural consequence of the symmetry concerning the right- to left-handed reversal of the rotational angular momentum and the polarisation of the probe pulse. At this delay time, all of the probed rotational states showed the same preference in the orientation, so that all of the observed transitions for $\Delta\phi = \pi/4$ $(-\pi/4)$ appeared to be stronger (weaker) for the right-handed probe than those for the opposite circularity. The TDSE calculation has also been performed to simulate the observation, by taking into account the initial distribution over the five different rotational levels (with 19 different M sublevels in total), as shown in the top panel of Figure 21. The match-up between the observed and calculated was satisfactory.

The delay dependence of the orientation was also examined numerically in [57]. The averaged degree of orientation, $\langle \hat{\mathbf{J}}_Z \rangle \equiv \langle \mathbf{J}_Z \rangle / \sqrt{\langle \mathbf{J}^2 \rangle}$, was evaluated by the TDSE calculation for the ensemble starting from the five levels and their nuclear-spin weighted average, as shown in Figure 22. The largest value of $|\langle \hat{\mathbf{J}}_Z \rangle|$ reaches to 0.6 for $(J, K) = (0, 0)$. The oscillation amplitude of $\langle \hat{\mathbf{J}}_Z \rangle$ gradually decreases for the initial rotational states with a larger J, mainly due to partial cancellation by contributions from different M sublevels.

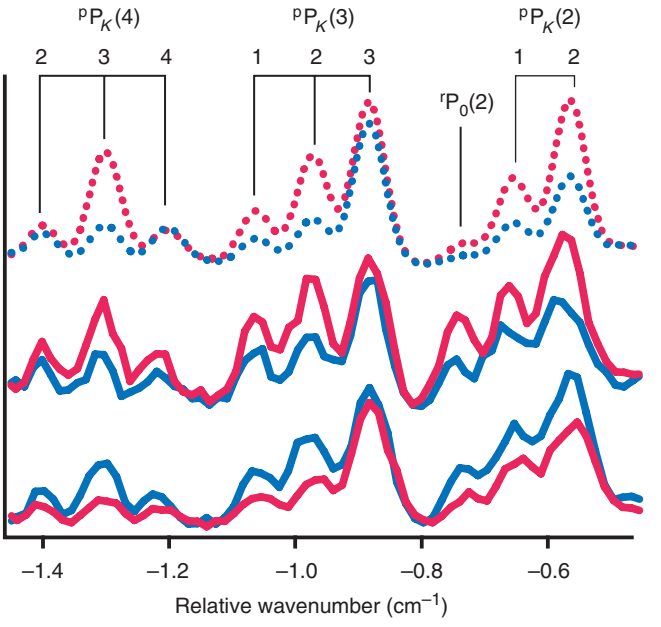

Figure 21. [Colour online] Excitation spectra of the P-branch region in the $S_1 \leftarrow S_0 6_0^1$ band of benzene after a fs double-pulse excitation with τ set to 7.3 ps, recorded with the right-handed (blue lines) and left-handed (red lines) polarised probe pulse. The middle and lower panels show experimentally observed ones for $\Delta\phi = -\pi/4$ and $\pi/4$, respectively, while the upper one is simulated for $\Delta\phi = -\pi/4$ with a laser peak intensity of 1.2 TW/cm^2 for each pulse. From Ref. [57].

Still, the gross average of the five states keeps the largest $|\langle\hat{\mathbf{J}}_Z\rangle|$ of ~0.2. $\langle\hat{\mathbf{J}}_Z\rangle$ for an ensemble of different J levels shows revival transients, exhibiting dispersion-like shapes with ~10 ps duration at around the multiples of the half revival time, $T_{\rm rev}/2 = 1/(4Bc)$. These transients look similar to those appearing in molecular-axis alignment and orientation [14–21,149,151]. In particular, $\langle\hat{\mathbf{J}}_Z\rangle$ in the vicinity of the zero delay rapidly reaches its maximum (or minimum) within +5 (or −5) ps, which is much shorter than the typical time scale of rotation, $T_{\rm rev}$.

It should be pointed out that the oriented states provided in this scheme are wave packets, or their ensembles with respect to the initially populated eigenstates, and thus exhibit spatiotemporal propagation in an ultrafast time regime, which is a quantum-mechanical representation of clockwise or counter-clockwise rotation of molecules. Such nonstationary microscopic states of unidirectionally circulating motion have rarely been realised, whereas time-dependent molecular alignment has been extensively studied so far. While the theoretical consideration mentioned above is totally in a quantum-mechanical perspective, Fleischer *et al.* [185] have shown that a classical explanation can also be given for controlling the sense of rotation by the two impulsive-pulse excitation. The classical description can be summarised as the following two successive processes. The first impulsive pulse imposes a torque to the initial molecular ensemble with an isotropic distribution, yielding to a squeezing of the angular distribution of the molecular axis along, or perpendicular to, the laser polarisation direction. Then, the second impulse after an

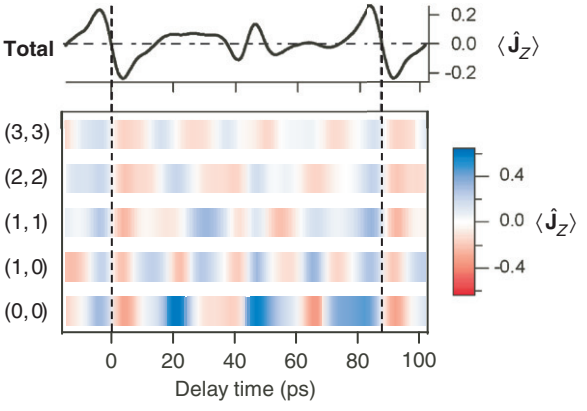

Figure 22. Delay-time dependence of the degree of orientation, $\langle \hat{\mathbf{J}}_Z \rangle$, for wave packets, created from the five lowest rotational levels $(J, K) = (0, 0)$, $(1, 0)$, $(1, 1)$, $(2, 2)$ and $(3, 3)$, as well as their nuclear-spin weighted average (total). The laser peak intensity is 1.2 TW/cm^2 for each pulse and $\Delta\phi$ is set to $-\pi/4$. Vertical broken lines indicate delay time at zero and $T_{\text{rev}} \sim 88$ ps. From Ref. [57].

appropriate delay time exerts another torque to align the molecular axis tilted by 45° from the direction of the foregoing angular squeezing, to give rise to a unidirectional rotation of the molecular ensemble. Here, the angular squeezing is a general phenomenon both in classical and quantum systems when the delay between the two pulses is not so large that the squeezing is achieved slightly after the impulse by the first pulse [117,118]. In this case the creation of a unidirectionally rotating molecular ensemble is totally within the classical perspective. On the other hand, angular squeezing can also be achieved after a longer delay at the times of the rotational revivals. Such a kind of revival is involved with quantisation of the rotational angular momentum, or the discrete nature of the rotational energy and a correlation (harmonic relation) in the energy-level structure. Then, the latter part in the two-step mechanism comes to invoke a quantum depiction. Fleischer *et al.* [185] have examined the relative power dependence on $\left|\langle \hat{\mathbf{J}}_Z \rangle\right|$ for a molecular ensemble in a thermal condition to show that $\left|\langle \hat{\mathbf{J}}_Z \rangle\right|$ is maximised when the two pulses have identical strength.

6. Outlook and conclusion

As demonstrated in Sections 5.1 and 5.2, the quantum-state-resolved probe pertinent to NAREX can provide indispensable insights into excitation by intense nonresonant ultrafast laser fields. The approach directly provides the diagonal elements of the density matrix describing the NAREX process, which are usually difficult to extract by the established methods for probing the degree of alignment. It is particularly beneficial when we attempt to evaluate various scenarios proposed recently for ultrafast population control *via* the manipulation of rotational wave packets [52,56–59]. Furthermore, the state-resolved approach allows us to determine the excitation pathways experimentally, when the double-pulse excitation is applied. Since the behaviours of diatomic/linear and symmetric-top molecules have already been examined, asymmetric-top molecules will be

explored next. The multidimensional character of such molecules has been the subject of substantial theoretical and experimental work [22–24,125,126]. In particular, it has recently been shown that the directional dynamics of asymmetric tops exhibit a distinct transition when the field strength of the excitation pulse is increased [126]. This new mode of spatiotemporal propagation of the rotational state will be detailed by state-resolved measurements. An experimental challenge is a serious spectral congestion frequently appearing in asymmetric-top molecules, and frequency resolution with commercially available dye lasers will not be sufficient. We may have to implement advanced laser systems (e.g. based on the pulsed amplification of single-mode cw laser outputs), which provide single-longitudinal-mode pulses with a Fourier-transform-limited bandwidth (typically well below $0.01\,\mathrm{cm}^{-1}$).

As mentioned in Section 2.4, there is a rapidly growing number of studies for the advanced control of rotational wave packets by implementing multiple-pulse excitation [128–130,132–136], or using highly sculptured pulses [139–152]. An experimental retrieval of the resultant quantum state is crucial for further wave-packet processing. Manipulations by NAREX are very sensitive to the light fields because of the highly nonlinear nature of the excitation processes, far beyond the perturbative regime in light–matter interactions. A precise determination of the light field at the interaction region is not easy, particularly for a sophisticatedly structured excitation pulse. In this context, the experimental reconstruction procedure described in Section 5.3 will become much more significant, since it can be applied to various types of molecule. The procedure can be extended to holographic reconstruction, which is similar to those developed for resonant excitations in a perturbative regime [177–179]. In wave-packet holography, an unknown 'target' state will interfere with a well-characterised 'reference' state. The population of the initial state is monitored after the interaction of the two successive (i.e. 'target' and 'reference') pulses. Then, the delay-dependent population is represented as

$$\left|B_{r_i,r_i}(\tau)\right|^2 = \sum_{r'} \left(A^{\mathrm{tar}}_{r_i,r'}\right)^2 \left(A^{\mathrm{ref}}_{r_i,r'}\right)^2 + 2 \sum_{r' > r''} A^{\mathrm{tar}}_{r_i,r'} A^{\mathrm{tar}}_{r_i,r''} A^{\mathrm{ref}}_{r_i,r'} A^{\mathrm{ref}}_{r_i,r''} \cos\left(\Delta\omega_{r',r''}\tau + \Delta\delta\right), \quad (54)$$

with

$$\Delta\delta = \delta^{\mathrm{tar}}_{r_i,r''} - \delta^{\mathrm{tar}}_{r_i,r'} + \delta^{\mathrm{ref}}_{r_i,r''} - \delta^{\mathrm{ref}}_{r_i,r'}. \quad (55)$$

Thus, all of the phases for the 'target' state can be determined unambiguously, with the aforementioned π uncertainty being eliminated. The 'reference' state can be prepared as that created *via* NAREX by a simple enveloped pulse, with the field strength estimated from the experimental beam parameters. Characterisation of the 'reference' state will be carried out by the procedure described in Section 5.3, in which the 'reference' pulse and its replica are used. After a determination of the 'reference', the replica will be replaced by the programmed pulse to sculpture a wave packet, yielding the holographic reconstruction of the 'target' state thus created.

There are many possibilities for further investigations on unidirectionally rotating wave packets. First, the degree of orientation can be improved by more elaborate excitation with, e.g. multiple pulses or shaped pulses. NAREX with a skewed linearly polarised pulse pair inherently involves excitation with $\Delta M = 0$, as can be clearly seen in Figure 20. If the excitation pathway is effectively cancelled out, the degree of orientation will be substantially increased. Second, control of angular momentum may be extended to

dense gases or even to some condensed media [186–189], when the turbulence from environments that brings the loss of coherence in the created wave packets is slower than the creation of orientation. Third, control of angular-momentum orientation is not necessarily restricted to the overall rotation of molecules. It may also be possible to orient the vibrational and/or electronic angular momentum in 2-D or 3-D isotropic systems, when the relevant energy intervals are small enough to be covered by the laser bandwidth. Such an angular-momentum orientation will be useful for ultrafast control of the magnetic and optical response of the ensemble under consideration.

When the intensity of the nonresonant ultrafast pulse is increased, the irradiated molecules are ionised as well as being rotationally excited. The strong-field ionisation has been shown to have a significant dependence on the alignment angle of the molecular axis with respect to the laser polarisation [30,35,40]. The population in the neutral state is angle-selectively depleted, resulting in the creation of a rotational wave packet. Similarly, it has been proposed and verified that internuclear-distance dependent depletion by strong-field ionisation creates a vibrational wave packet in the neutral ground state [190,191]. The alignment-dependent ionisation and the NAREX occur simultaneously with a certain extent of coherent correlation, and they cannot be treated as independent processes. Quite recently, the rotational-state distribution of neutral NO molecules surviving strong-field ionisation have been explored experimentally and theoretically to assess the correlated dynamics [192]. It is certainly possible to extend these studies, e.g. by a thorough examination of the intensity and the pulse-duration dependences and by implementation of the wave-packet reconstruction mentioned just above.

Since the polarisability of a molecule usually varies as its geometrical structure is deformed, the field–matter interaction represented in Equation (1) depends not only on the rotational coordinates (i.e. Euler angles), but also on the vibrational coordinates. Thus, nonadiabatic interactions with a nonresonant ultrafast laser field can coherently excite molecular vibration. The realisation of such a nonadiabatic vibrational excitation (NAVEX) and the resultant creation of a vibrational wave packet is definitely the next step to be made. Indeed, there have already been several reports of the observation of the real-time propagation of vibrational wave packets induced by an impulsive excitation with nonresonant intense fs pulses. HHG was applied to SF_6 and N_2O_4, for which the vibrational coherence created by a fundamental output from a Ti:sapphire laser was monitored as the modulation of the high harmonics by the delayed second pulse [193,194]. An ion-imaging technique has been used for real-time probing the torsional motion of a substituted biphenyl molecule, in which the molecular axis was fixed in space by adiabatic alignment [195]. The quantum-state resolved approach with ns probe pulses will also contribute to the research of nonadiabatic excitation of molecular vibration. It provides several advantages, as in the case of studies on NAREX described in the previous sections. First of all, the REMPI probe adopted herein provides an unambiguous selection of molecular species by specifying the resonant transition and the ion mass channel to be monitored. The vibronic band selection also ensures that the coherent transients observed are exclusively those in the ground-state manifold. In addition, since the vibrational excitation is attained by nonresonant impulsive pulses with a fixed wavelength, the method will be applicable to various molecular systems once they have vibronic transitions suitable to the REMPI probe. The best candidates for the state-selective approach are Van der Waals (VdW) clusters, weakly bound by intermolecular interactions. In studies of neutral

clusters, the duplex selection in mass channel and probe wavelength is crucial for a definite size assignment, while the conventional ultrafast pump–probe approach often suffers from mass channel chattering by fragmentation after ionisation. Because of the weak anisotropy of the intermolecular forces, librations of constituent molecules in VdW clusters are highly anharmonic and have wide amplitudes. Such intermolecular motions are inherently associated with large modulation of polarisability, which is attached to the constituent molecules. Accordingly, VdW clusters, particularly those composed of molecules with large anisotropic polarisability, are expected to show strong Raman activities for low-frequency intermolecular modes, as has been shown experimentally [164,165]. Time-domain studies will directly map out energy-level intervals and transition probabilities pertinent to intermolecular vibration, as the frequency-domain experiments have been doing [164,165]. One of the plausible advances from using intense ultrafast pulses is multi-step Raman excitation to high lying levels, which are often difficult to access from the zero-point level *via* a single Raman transition. Such a coherent excitation will be a milestone in wave-packet manipulation of intermolecular vibration, with the ultimate goal being coherent control of conformational transformations in floppy systems.

Acknowledgements

We thank Drs Kenta Kitano and Daeyul Baek for their contributions to the NAREX studies carried out in the Institute for Molecular Science. Valuable discussions on the unidirectionally rotating wave packets with Profs. Ilya Averbukh and Yehiam Prior are gratefully acknowledged. We also appreciate the financial support provided for our NAREX research by Grants-in-Aid from MEXT, the RIKEN-IMS joint programme on 'Extreme Photonics', and Consortium for Photon Science and Technology.

References

[1] http://nobelprize.org/nobel_prizes/physics/laureates/2001/index.html
[2] L. Pitaevskii and S. Stringari, *Bose–Einstein Condensation* (Oxford University Press, Oxford, 2003).
[3] K.-K. Ni, S. Ospelkaus, D. J. Nesbitt, J. Ye, and D. S. Jin, Phys. Chem. Chem. Phys. **11**, 9626 (2009).
[4] S. Y. T. van de Meerakker, H. L. Bethlem, and G. Meijer, Nat. Phys. **4**, 595 (2008).
[5] R. D. Levine and R. B. Bernstein, *Molecular Reaction Dynamics and Chemical Reactivity* (Oxford University Press, New York, 1987).
[6] K. T. Lorenz, D. W. Chandler, J. W. Barr, W. Chen, G. L. Barnes, and J. I. Cline, Science **293**, 2063 (2001).
[7] F. Pirani, M. Bartolomei, V. Aqulanti, M. Scotoni, M. Vescovi, D. Ascenzi, D. Bassi, and D. Cappelletti, J. Chem. Phys. **119**, 265 (2003).
[8] D. H. Parker and R. B. Bernstein, Annu. Rev. Phys. Chem. **40**, 561 (1989).
[9] B. Friedrich and D. R. Herschbach, Z. Phys. D **18**, 153 (1991).
[10] H. J. Loesch and A. Remscheid, J. Chem. Phys. **93**, 4779 (1990).
[11] H. J. Loesch, Annu. Rev. Phys. Chem. **46**, 555 (1995).
[12] C. H. Greene and R. N. Zare, Annu. Rev. Phys. Chem. **33**, 119 (1982).
[13] W. Happer, Rev. Mod. Phys. **44**, 169 (1972).
[14] H. Stapelfeldt and T. Seideman, Rev. Mod. Phys. **75**, 543 (2003).
[15] T. Seideman and E. Hamilton, Adv. At. Mol. Opt. Phys. **52**, 289 (2005).

[16] T. Seideman, J. Chem. Phys. **103**, 7887 (1995).
[17] T. Seideman, Phys. Rev. Lett. **83**, 4971 (1999).
[18] J. Ortigoso, M. Rodríguez, M. Gupta, and B. Friedrich, J. Chem. Phys. **110**, 3870 (1999).
[19] F. Rosca-Pruna and M. J. J. Vrakking, Phys. Rev. Lett. **87**, 153902 (2001).
[20] F. Rosca-Pruna and M. J. J. Vrakking, J. Chem. Phys. **116**, 6567, 6579 (2002).
[21] P. W. Dooley, I. V. Litvinyuk, K. F. Lee, D. M. Rayner, M. Spanner, D. M. Villeneuve, and P. B. Corkum, Phys. Rev. A **68**, 023406 (2003).
[22] E. Péronne, M. D. Poulsen, C. Z. Bisgaard, H. Stapelfeldt, and T. Seideman, Phys. Rev. Lett. **91**, 043003 (2003).
[23] M. D. Poulsen, E. Péronne, H. Stapelfeldt, C. Z. Bisgaard, S. S. Viftrup, E. Hamilton, and T. Seideman, J. Chem. Phys. **121**, 783 (2004).
[24] E. Péronne, M. D. Poulsen, H. Stapelfeldt, C. Z. Bisgaard, E. Hamilton, and T. Seideman, Phys. Rev. A **70**, 063410 (2004).
[25] E. Hamilton, T. Seideman, T. Ejdrup, M. D. Poulsen, C. Z. Bisgaard, S. S. Viftrup, and H. Stapelfeldt, Phys. Rev. A **72**, 043402 (2005).
[26] K. Miyazaki, M. Kaku, G. Miyaji, A. Abdurrouf, and F. H. M. Faisal, Phys. Rev. Lett. **95**, 243903 (2005).
[27] V. Renard, M. Renard, S. Guérin, Y. T. Pashayan, B. Lavorel, O. Faucher, and H. R. Jauslin, Phys. Rev. Lett. **90**, 153601 (2003).
[28] M. Comstock, V. Senekerimyan, and M. Dantus, J. Phys. Chem. A **107**, 8271 (2003).
[29] V. G. Stavros, E. Harel, and S. R. Leone, J. Chem. Phys. **122**, 064301 (2005).
[30] I. V. Litvinyuk, K. F. Lee, P. W. Dooley, D. M. Rayner, D. M. Villeneuve, and P. B. Corkum, Phys. Rev. Lett. **90**, 233003 (2003).
[31] M. Spanner, E. A. Shapiro, and M. Ivanov, Phys. Rev. Lett. **92**, 093001 (2004).
[32] K. F. Lee, D. M. Villeneuve, P. B. Corkum, and E. A. Shapiro, Phys. Rev. Lett. **93**, 233601 (2004).
[33] J. Itatani, J. Levesque, D. Zeidler, H. Niikura, H. Pépin, J. C. Kieffer, P. B. Corkum, and D. M. Villeneuve, Nature **432**, 867 (2004).
[34] T. Kanai, S. Minemoto, and H. Sakai, Nature **435**, 470 (2005).
[35] D. Zeidler, A. Staudte, A. B. Bardon, D. M. Villeneuve, R. Dörner, and P. B. Corkum, Phys. Rev. Lett. **95**, 203003 (2005).
[36] K. F. Lee, E. A. Shapiro, D. M. Villeneuve, and P. B. Corkum, Phys. Rev. A **73**, 033403 (2006).
[37] S. Fleischer, I. Sh. Averbukh, and Y. Prior, Phys. Rev. A **74**, 041403 (2006).
[38] S. Fleischer, I. Sh. Averbukh, and Y. Prior, Phys. Rev. Lett. **99**, 093002 (2007).
[39] R. Torres, N. Kajumba, J. G. Underwood, J. S. Robinson, S. Baker, J. W. G. Tisch, R. de Nalda, W. A. Bryan, R. Velotta, C. Altucci, I. C. E. Turcu, and J. P. Marangos, Phys. Rev. Lett. **98**, 203007 (2007).
[40] D. Pavičić, K. F. Lee, D. M. Rayner, P. B. Corkum, and D. M. Villeneuve, Phys. Rev. Lett. **98**, 243001 (2007).
[41] J. Levesque, Y. Mairesse, N. Dudovich, H. Pépin, J.-C. Kieffer, P. B. Corkum, and D. M. Villeneuve, Phys. Rev. Lett. **99**, 243001 (2007).
[42] N. Wagner, X. Zhou, R. Lock, W. Li, A. Wüest, M. Murnane, and H. Kapteyn, Phys. Rev. A **76**, 061403 (2007).
[43] M. Meckel, D. Comtois, D. Zeidler, A. Staudte, D. Pavičić, H. C. Bandulet, H. Pépin, J. C. Kieffer, R. Dörner, D. M. Villeneuve, and P. B. Corkum, Science **320**, 478 (2008).
[44] W. Boutu, S. Haessler, H. Merdji, P. Breger, G. Waters, M. Stankiewicz, L. J. Frasinski, R. Taieb, J. Caillat, A. Maquet, P. Monchicourt, B. Carre, and P. Salieres, Nat. Phys. **4**, 545 (2008).
[45] V. Kumarappan, L. Holmegaard, C. Martiny, C. B. Madsen, T. K. Kjeldsen, S. S. Viftrup, L. B. Madsen, and H. Stapelfeldt, Phys. Rev. Lett. **100**, 093006 (2008).

[46] Y. Mairesse, D. Zeidler, N. Dudovich, M. Spanner, J. Levesque, D. M. Villeneuve, and P. B. Corkum, Phys. Rev. Lett. **100**, 143903 (2008).
[47] S. Minemoto, T. Kanai, and H. Sakai, Phys. Rev. A **77**, 041401 (2008).
[48] T. Kanai, E. J. Takahashi, Y. Nabekawa, and K. Midorikawa, Phys. Rev. A **77**, 041402 (2008).
[49] O. Smirnova, Y. Mairesse, S. Patchkovskii, N. Dudovich, D. Villeneuve, P. Corkum, and M. Yu. Ivanov, Nature **460**, 972 (2009).
[50] O. Smirnova, S. Patchkovskii, Y. Mairesse, N. Dudovich, D. M. Villeneuve, P. B. Corkum, and M. Yu. Ivanov, Phys. Rev. Lett. **102**, 063601 (2009).
[51] H. Hasegawa and Y. Ohshima, Phys. Rev. A **74**, 061401 (2006).
[52] A. S. Meijer, Y. Zhang, D. H. Parker, W. J. van der Zande, A. Gijsbertsen, and M. J. J. Vrakking, Phys. Rev. A **76**, 023411 (2007).
[53] H. Hasegawa and Y. Ohshima, Chem. Phys. Lett. **454**, 148 (2008).
[54] H. Hasegawa and Y. Ohshima, Phys. Rev. Lett. **101**, 053002 (2008).
[55] H. Hasegawa and Y. Ohshima, Proc. SPIE Int. Soc. Opt. Eng. **7027**, 70271F (2008).
[56] H. Hasegawa and Y. Ohshima, J. Phys. Conf. Ser. **185**, 012014 (2009).
[57] K. Kitano, H. Hasegawa, and Y. Ohshima, Phys. Rev. Lett. **103**, 223002 (2009).
[58] C. Wu, G. Zeng, Y. Gao, N. Xu, L.-Y. Peng, H. Jiang, and Q. Gong, J. Chem. Phys. **130**, 231102 (2009).
[59] Y. Li, P. Liu, S. Zhao, Z. Zeng, R. Li, and Z. Xu, Chem. Phys. Lett. **475**, 183 (2009).
[60] S. Zhao, P. Liu, Y. Li, R. Li, and Z. Xu, Chem. Phys. Lett. **480**, 67 (2009).
[61] N. Owschimikow, B. Schmidt, and N. Schwentner, Phys. Rev. A **80**, 053409 (2009).
[62] T. P. Rakitzis, A. J. van den Brom, and M. H. M. Janssen, Science **303**, 1852 (2004).
[63] H. Ohoyama, F. Kubo, and T. Kasai, J. Chem. Phys. **131**, 134306 (2009).
[64] A. Gijsbertsen, W. Siu, M. F. Kling, P. Johnsson, P. Jansen, S. Stolte, and M. J. J. Vrakking, Phys. Rev. Lett. **99**, 213003 (2007).
[65] K. J. Franks, H. Li, and W. Kong, J. Chem. Phys. **111**, 1884 (1999).
[66] K. J. Castle, J. Abbott, X. Peng, and W. Kong, J. Chem. Phys. **113**, 1415 (2000).
[67] L. Oudejans and R. E. Miller, J. Chem. Phys. **113**, 4581 (2000).
[68] K. Nauta and R. E. Miller, Science **283**, 1895 (1999).
[69] F. Dong and R. E. Miller, Science **298**, 1227 (2002).
[70] R. Kanya and Y. Ohshima, Chem. Phys. Lett. **370**, 211 (2003).
[71] R. Kanya and Y. Ohshima, J. Chem. Phys. **121**, 9489 (2004).
[72] R. Kanya and Y. Ohshima, Phys. Rev. A **70**, 013403 (2004).
[73] J. Bulthuis, J. Möller, and H. J. Loesch, J. Phys. Chem. A **101**, 7684 (1997).
[74] W. Kong and J. Bulthuis, J. Phys. Chem. A **104**, 1055 (2000).
[75] R. N. Zare, *Angular Momentum* (Wiley, New York, 1988), Chap. 5.
[76] K. Blum, *Density Matrix Theory and Applications* (Plenum, New York, 1996), Chap. 7.
[77] N. C.-M. Bartlett, D. J. Miller, R. N. Zare, A. J. Alexander, D. Sofikitis, and T. P. Rakitzis, Phys. Chem. Chem. Phys. **11**, 142 (2009); also see references cited therein.
[78] R. Neuhauser and H. J. Neusser, J. Chem. Phys. **103**, 5362 (1995).
[79] J. Qi, G. Lazarov, X. Wang, L. Li, L. M. Narducci, A. M. Lyyra, and F. C. Spano, Phys. Rev. Lett. **83**, 288 (1999).
[80] B. Friedrich and D. R. Herschbach, Phys. Rev. Lett. **74**, 4623 (1995).
[81] B. Friedrich and D. R. Herschbach, J. Phys. Chem. **99**, 15686 (1995).
[82] W. Kim and P. M. Felker, J. Chem. Phys. **104**, 1147 (1996).
[83] W. Kim and P. M. Felker, J. Chem. Phys. **107**, 2193 (1997).
[84] W. Kim and P. M. Felker, J. Chem. Phys. **108**, 6763 (1998).
[85] H. Sakai, C. P. Safvan, J. J. Larsen, K. M. Hilligsøe, K. Hald, and H. Stapelfeldt, J. Chem. Phys. **110**, 10235 (1999).
[86] J. J. Larsen, H. Sakai, C. P. Safvan, I. Wendt-Larsen, and H. Stapelfeldt, J. Chem. Phys. **111**, 7774 (1999).

[87] J. J. Larsen, I. Wendt-Larsen, and H. Stapelfeldt, Phys. Rev. Lett. **83**, 1123 (1999).
[88] A. Sugita, M. Mashino, M. Kawasaki, Y. Matsumi, R. J. Gordon, and R. Bersohn, J. Chem. Phys. **112**, 2164 (2000).
[89] M. D. Poulsen, E. Skovsen, and H. Stapelfeldt, J. Chem. Phys. **117**, 2097 (2002).
[90] S. Minemoto, H. Tanji, and H. Sakai, J. Chem. Phys. **119**, 7737 (2003).
[91] A. Iwasaki, A. Hishikawa, and K. Yamanouchi, Chem. Phys. Lett. **346**, 379 (2001).
[92] K. Hoshina, K. Yamanouchi, T. Ohshima, Y. Ose, and H. Todokoro, Chem. Phys. Lett. **353**, 27, 33 (2002).
[93] K. Hoshina, K. Yamanouchi, T. Ohshima, Y. Ose, and H. Todokoro, J. Chem. Phys. **118**, 6211 (2003).
[94] M. Artamonov and T. Seideman, J. Chem. Phys. **128**, 154313 (2008).
[95] J. J. Larsen, K. Hald, N. Bjerre, H. Stapelfeldt, and T. Seideman, Phys. Rev. Lett. **85**, 2470 (2000).
[96] B. Friedrich and D. R. Herschbach, J. Phys. Chem. A **103**, 10280 (1999).
[97] B. Friedrich and D. R. Herschbach, J. Chem. Phys. **111**, 6157 (1999).
[98] M. Härtelt and B. Friedrich, J. Chem. Phys. **128**, 224313 (2008).
[99] H. Sakai, S. Minemoto, H. Nanjo, H. Tanji, and T. Suzuki, Phys. Rev. Lett. **90**, 083001 (2003).
[100] H. Tanji, S. Minemoto, and H. Sakai, Phys. Rev. A **72**, 063401 (2005).
[101] N. H. Nahler, R. Baumfalk, U. Buck, Z. Bihary, R. B. Gerber, and B. Friedrich, J. Chem. Phys. **119**, 224 (2003).
[102] U. Buck and M. Fárník, Int. Rev. Phys. Chem. **25**, 583 (2006).
[103] V. Poterya, O. Votava, M. Fárník, M. Ončák, P. Slavíček, U. Buck, and B. Friedrich, J. Chem. Phys. **128**, 104313 (2008).
[104] S. Minemoto, H. Nanjo, H. Tanji, T. Suzuki, and H. Sakai, J. Chem. Phys. **118**, 4052 (2003).
[105] V. Kumarappan, C. Z. Bisgaard, S. S. Viftrup, L. Holmegaard, and H. Stapelfeldt, J. Chem. Phys. **125**, 194309 (2006).
[106] L. Holmegaard, J. H. Nielsen, I. Nevo, H. Stapelfeldt, F. Filsinger, J. Küpper, and G. Meijer, Phys. Rev. Lett. **102**, 023001 (2009).
[107] F. Filsinger, J. Küpper, G. Meijer, L. Holmegaard, J. H. Nielsen, I. Nevo, J. L. Hansen, and H. Stapelfeldt, J. Chem. Phys. **131**, 064309 (2009).
[108] I. Nevo, L. Holmegaard, J. H. Nielsen, J. L. Hansen, H. Stapelfeldt, F. Filsinger, G. Meijer, and J. Küpper, Phys. Chem. Chem. Phys. **11**, 9912 (2009).
[109] T. Kanai and H. Sakai, J. Chem. Phys. **115**, 5492 (2001).
[110] K. Oda, M. Hita, S. Minemoto, and H. Sakai, Phys. Rev. Lett. **104**, 213901 (2010).
[111] C. H. Lin, J. P. Heritage, and T. K. Gustafson, Appl. Phys. Lett. **19**, 397 (1971).
[112] J. P. Heritage, T. K. Gustafson, and C. H. Lin, Phys. Rev. Lett. **34**, 1299 (1975).
[113] J. S. Baskin and A. H. Zewail, J. Phys. Chem. **93**, 5701 (1989).
[114] P. Felker and A. H. Zewail, J. Chem. Phys. **86**, 2460 (1987).
[115] J. S. Baskin, P. Felker, and A. H. Zewail, J. Chem. Phys. **86**, 2483 (1987).
[116] T. Seideman, J. Chem. Phys. **115**, 5965 (2001).
[117] I. Sh. Averbukh and R. Arvieu, Phys. Rev. Lett. **87**, 163601 (2001).
[118] M. Leibscher, I. Sh. Averbukh, and H. Rabitz, Phys. Rev. Lett. **90**, 213001 (2003).
[119] D. Pinkham and R. R. Jones, Phys. Rev. A **72**, 023418 (2005).
[120] W. A. Bryan, E. M. L. English, J. McKenna, J. Wood, C. R. Calvert, I. C. E. Turcu, R. Torres, J. L. Collier, I. D. Williams, and W. R. Newell, Phys. Rev. A **76**, 023414 (2007).
[121] I. A. Bocharova, H. Mashiko, M. Magrakvelidze, D. Ray, P. Ranitovic, C. L. Cocke, and I. V. Litvinyuk, Phys. Rev. A **77**, 053407 (2008).
[122] D. W. Broege, R. N. Coffee, and P. H. Bucksbaum, Phys. Rev. A **78**, 035401 (2008).
[123] A. Rouzée, V. Renard, S. Guérin, O. Faucher, and B. Lavorel, Phys. Rev. A **75**, 013419 (2007).
[124] Y. Gao, C. Wu, N. Xu, G. Zeng, H. Jiang, H. Yang, and Q. Gong, Phys. Rev. A **77**, 043404 (2008).

[125] A. Rouzée, S. Guérin, V. Boudon, B. Lavorel, and O. Faucher, Phys. Rev. A **73**, 033418 (2006).
[126] L. Holmegaard, S. S. Viftrup, V. Kumarappan, C. Z. Bisgaard, H. Stapelfeldt, E. Hamilton, and T. Seideman, Phys. Rev. A **75**, 051403 (2007).
[127] E. A. Torres, E.-B. W. Lerch, X. Dai, S. Gilb, and S. R. Leone, J. Chem. Phys. **126**, 044310 (2007).
[128] C. Z. Bisgaard, M. D. Poulsen, E. Péronne, S. S. Viftrup, and H. Stapelfeldt, Phys. Rev. Lett. **92**, 173004 (2004).
[129] C. Z. Bisgaard, S. S. Viftrup, and H. Stapelfeldt, Phys. Rev. A **73**, 053410 (2006).
[130] J. P. Cryan, P. H. Bucksbaum, and R. N. Coffee, Phys. Rev. A **80**, 063412 (2009).
[131] E. Gershnabel and I. Sh. Averbukh, Phys. Rev. A **78**, 063416 (2008).
[132] J. G. Underwood, B. J. Sussman, and A. Stolow, Phys. Rev. Lett. **94**, 143002 (2005).
[133] K. F. Lee, D. M. Villeneuve, P. B. Corkum, A. Stolow, and J. G. Underwood, Phys. Rev. Lett. **97**, 173001 (2006).
[134] M. D. Poulsen, T. Ejdrup, H. Stapelfeldt, E. Hamilton, and T. Seideman, Phys. Rev. A **73**, 033405 (2006).
[135] S. S. Viftrup, V. Kumarappan, S. Trippel, H. Stapelfeldt, E. Hamilton, and T. Seideman, Phys. Rev. Lett. **99**, 143602 (2007).
[136] S. S. Viftrup, V. Kumarappan, L. Holmegaard, C. Z. Bisgaard, H. Stapelfeldt, M. Artamonov, E. Hamilton, and T. Seideman, Phys. Rev. A **79**, 023404 (2009).
[137] E. Hertz, D. Daems, S. Guérin, H. R. Jauslin, B. Lavorel, and O. Faucher, Phys. Rev. A **76**, 043423 (2007).
[138] A. Rouzée, S. Guérin, O. Faucher, and B. Lavorel, Phys. Rev. A **77**, 043412 (2008).
[139] J. G. Underwood, M. Spanner, M. Y. Ivanov, J. Mottershead, B. J. Sussman, and A. Stolow, Phys. Rev. Lett. **90**, 223001 (2003).
[140] B. J. Sussman, J. G. Underwood, R. Lausten, M. Y. Ivanov, and A. Stolow, Phys. Rev. A **73**, 053403 (2006).
[141] M. Renard, E. Hertz, B. Lavorel, and O. Faucher, Phys. Rev. A **69**, 043401 (2004).
[142] M. Renard, E. Hertz, S. Guérin, H. R. Jauslin, B. Lavorel, and O. Faucher, Phys. Rev. A **72**, 025401 (2005).
[143] C. Horn, M. Wollenhaupt, M. Krug, T. Baumert, R. de Nalda, and L. Bañares, Phys. Rev. A **73**, 031401 (2006).
[144] E. Hertz, A. Rouzée, S. Guérin, B. Lavorel, and O. Faucher, Phys. Rev. A **75**, 031403 (2007).
[145] D. Pinkham, K. E. Mooney, and R. R. Jones, Phys. Rev. A **75**, 013422 (2007).
[146] T. Suzuki, Y. Sugawara, S. Minemoto, and H. Sakai, Phys. Rev. Lett. **100**, 033603 (2008).
[147] J. Karczmarek, J. Wright, P. Corkum, and M. Ivanov, Phys. Rev. Lett. **82**, 3420 (1999).
[148] D. M. Villeneuve, S. A. Aseyev, P. Dietrich, M. Spanner, M. Yu. Ivanov, and P. B. Corkum, Phys. Rev. Lett. **85**, 542 (2000).
[149] M. Spanner and M. Yu. Ivanov, J. Chem. Phys. **114**, 3456 (2001).
[150] Y. Sugawara, A. Goban, S. Minemoto, and H. Sakai, Phys. Rev. A **77**, 031403 (2008).
[151] A. Goban, S. Minemoto, and H. Sakai, Phys. Rev. Lett. **101**, 013001 (2008).
[152] S. De, I. Znakovskaya, D. Ray, F. Anis, N. G. Johnson, I. A. Bocharova, M. Magrakvelidze, B. D. Esry, C. L. Cocke, I. V. Litvinyuk, and M. F. Kling, Phys. Rev. Lett. **103**, 153002 (2009).
[153] O. Ghafur, A. Rouzée, A. Gijsbertsen, W. K. Siu, S. Stolte, and M. J. J. Vrakking, Nat. Phys. **5**, 289 (2009).
[154] A. Rouzée, A. Gijsbertsen, O. Ghafur, O. M. Shir, T. Bäck, S. Stolte, and M. J. J. Vrakking, New J. Phys. **11**, 105040 (2009).
[155] V. Loriot, R. Tehini, E. Hertz, B. Lavorel, and O. Faucher, Phys. Rev. A **78**, 013412 (2008).
[156] A.-T. Le, R. R. Lucchese, M. T. Lee, and C. D. Lin, Phys. Rev. Lett. **102**, 203001 (2009).
[157] P. Johnsson, A. Rouzée, W. Siu, Y. Huismans, F. Lépine, T. Marchenko, S. Düsterer, F. Tavella, N. Stojanovic, A. Azima, R. Treusch, M. F. Kling, and M. J. J. Vrakking, J. Phys. B: At. Mol. Opt. Phys. **42**, 134017 (2009).

[158] F. H. M. Faisal, A. Abdurrouf, K. Miyazaki, and G. Miyaji, Phys. Rev. Lett. **98**, 143001 (2007).
[159] F. H. M. Faisal and A. Abdurrouf, Phys. Rev. Lett. **100**, 123005 (2008).
[160] K. Yoshii, G. Miyaji, and K. Miyazaki, Phys. Rev. Lett. **101**, 183902 (2008).
[161] A. Abdurrouf and F. H. M. Faisal, Phys. Rev. A **79**, 023405 (2009).
[162] K. Ohmori, Y. Sato, E. E. Nikitin, and S. A. Rice, Phys. Rev. Lett. **91**, 243003 (2003).
[163] K. Ohmori, H. Katsuki, H. Chiba, M. Honda, Y. Hagihara, K. Fujiwara, Y. Sato, and K. Ueda, Phys. Rev. Lett. **96**, 093002 (2006).
[164] G. V. Hartland, B. F. Henson, V. A. Venturo, R. A. Hertz, and P. M. Felker, J. Opt. Soc. Am. B **7**, 1950 (1990).
[165] P. M. Felker, P. M. Maxton, and M. W. Schaeffer, Chem. Rev. **94**, 1787 (1994).
[166] G. V. Hartland and P. M. Felker, J. Phys. Chem. **91**, 5527 (1987).
[167] G. V. Hartland, B. F. Henson, L. L. Connell, T. C. Corcoran, and P. M. Felker, J. Phys. Chem. **92**, 6877 (1988).
[168] S. M. Beck, M. G. Liverman, D. L. Monts, and R. E. Smalley, J. Chem. Phys. **70**, 232 (1979).
[169] A. L. L. East, H. Liu, E. C. Lim, P. Jensen, I. Déchène, M. Z. Zgierski, W. Siebrand, and P. R. Bunker, J. Chem. Phys. **112**, 167 (2000).
[170] J. P. Darr, R. A. Loomis, and A. B. McCoy, J. Chem. Phys. **122**, 044318 (2005).
[171] U. Even, J. Jortner, D. Noy, N. Lavie, and C. Cossart-Magos, J. Chem. Phys. **112**, 8068 (2000).
[172] J. Danielak, U. Domin, R. Kępa, M. Rytel, and M. Zachwieja, J. Mol. Spectrosc. **181**, 394 (1997).
[173] H. Hasegawa and Y. Ohshima (in preparation).
[174] D. Baek, H. Hasegawa, and Y. Ohshima (in preparation).
[175] M. Shapiro, J. Chem. Phys. **103**, 1748 (1995).
[176] I. Sh. Averbukh, M. Shapiro, C. Leichtle, and W. P. Schleich, Phys. Rev. A **59**, 2163 (1999).
[177] A. Zucchetti, W. Vegel, D.-G. Welsch, and I. A. Walmsley, Phys. Rev. A **60**, 2716 (1999).
[178] T. J. Dunn, I. A. Walmsley, and S. Mukamel, Phys. Rev. Lett. **74**, 884 (1995).
[179] T. C. Weinacht, J. Ahn, and P. H. Bucksbaum, Phys. Rev. Lett. **80**, 5508 (1998); Nature **397**, 233 (1999).
[180] E. Skovsen, H. Stapelfeldt, S. Juhl, and K. Mølmer, Phys. Rev. Lett. **91**, 090406 (2003).
[181] A. Monmayrant, B. Chatel, and B. Girard, Phys. Rev. Lett. **96**, 103002 (2006).
[182] P. F. Tekavec, T. R. Dyke, and A. H. Marcus, J. Chem. Phys. **125**, 194303 (2006).
[183] A. S. Mouritzen and K. Mølmer, J. Chem. Phys. **124**, 244311 (2006).
[184] Y. Kida, S. Zaitsu, and T. Imasaka, Phys. Rev. A **80**, 021805 (2009).
[185] S. Fleischer, Y. Khodorkovsky, Y. Prior, and I. Sh. Averbukh, New J. Phys. **11**, 105039 (2009).
[186] T. Kiljunen, B. Schmidt, and N. Schwentner, Phys. Rev. Lett. **94**, 123003 (2005); J. Chem. Phys. **124**, 164502 (2006).
[187] S. Ramakrishna and T. Seideman, Phys. Rev. Lett. **95**, 113001 (2005).
[188] D. Sugny, C. Kontz, and H. R. Jauslin, Phys. Rev. A **74**, 053411 (2006).
[189] A. Pelzer, S. Ramakrishna, and T. Seideman, J. Chem. Phys. **129**, 134301 (2008).
[190] E. Goll, G. Wunner, and A. Saenz, Phys. Rev. Lett. **97**, 103003 (2006).
[191] Th. Ergler, B. Feuerstein, A. Rudenko, K. Zrost, C. D. Schröter, R. Moshammer, and J. Ullrich, Phys. Rev. Lett. **97**, 103004 (2006).
[192] R. Itakura, H. Hasegawa, Y. Kurosaki, A. Yokoyama, and Y. Ohshima, J. Phys. Chem. A (in press).
[193] N. L. Wagner, A. Wüest, I. P. Christov, T. Popmintchev, X. Zhou, M. M. Murnane, and H. C. Kapteyn, Proc. Nat. Acad. Sci. U.S.A. **103**, 13279 (2006).
[194] W. Li, X. Zhou, R. Lock, S. Patchkovskii, A. Stolow, M. M. Murnane, and H. C. Kapteyn, Science **322**, 1207 (2008).
[195] C. B. Madsen, L. B. Madsen, S. S. Viftrup, M. P. Johansson, T. B. Poulsen, L. Holmegaard, V. Kumarappan, K. A. Jørgensen, and H. Stapelfeldt, Phys. Rev. Lett. **102**, 073007 (2009); J. Chem. Phys. **130**, 234310 (2009).